ACS OMEGA

Open Access

http://pubs.acs.org/journal/acsodf

Article

Selectivity Mechanism of Pyrrolopyridone Analogues Targeting Bromodomain 2 of Bromodomain-Containing Protein 4 from Molecular Dynamics Simulations

Mingsong Shi, Xueting Zheng, Yan Zhou, Yuan Yin, Zhou Lu, Zhiyan Zou, Yan Hu, Yuanyuan Liang, Tingting Chen, Yuhan Yang, Meng Jing, Dan Lei, Pei Yang,* and Xiaoan Li*

Cite This: *ACS Omega* 2023, 8, 33658−33674

Read Online

ACCESS | Metrics & More | Article Recommendations | Supporting Information

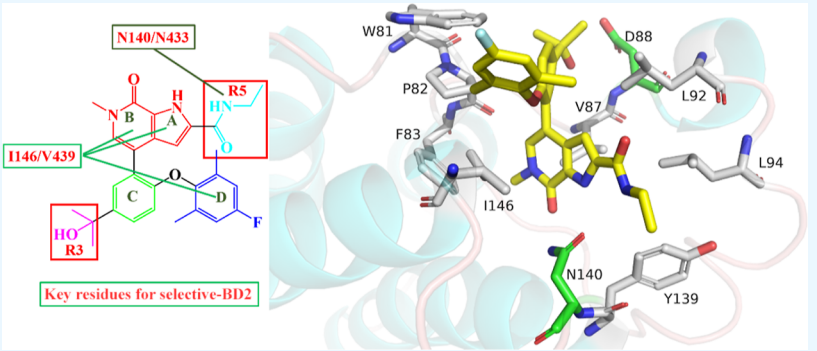

ABSTRACT: Bromodomain and extra-terminal domain (BET) proteins play an important role in epigenetic regulation and are linked to several diseases; therefore, they are interesting targets. BET has two bromodomains: bromodomain 1 (BD1) and BD2. Selective targeting of BD1 or BD2 may produce different activities and greater effects than pan-BD inhibitors. However, the selective mechanism of the specific core must be studied at the atomic level. This study determined the effectiveness of pyrrolopyridone analogues to selectively inhibit BD2 using a pan-BD inhibitor (ABBV-075) and a selective-BD2 inhibitor (ABBV-744). Molecular dynamics simulations and calculations of binding free energies were used to systematically study the selectivity of BD2 inhibition by the pyrrolopyridone analogues. Overall, the pyrrolopyridone analogue inhibitors targeting BD2 interacted mainly with the following amino acid pairs between bromodomain-containing protein 4 (BRD4)-BD1 and BRD4-BD2 complexes: I146/V439, N140/N433, D144/H437, P82/P375, V87/V380, D88/D381, and Y139/Y432. The pyrrolopyridone analogues targeting BRD4-BD2 were divided into five regions based on selectivity mechanism. These results suggest that the R3 and R5 regions of pyrrolopyridone analogues can be modified to improve the selectivity between BRD4-BD1 and BRD4-BD2. The selectivity of BD2 inhibition by pyrrolopyridone analogues can be used to design novel BD2 inhibitors based on a pyrrolopyridone core.

1. INTRODUCTION

Bromodomain and extra-terminal domain (BET) proteins play an important role in epigenetic regulation and are linked to several diseases, including acute liver injury,[1−3] acute myeloid leukemia,[4] triple negative breast cancer,[5−7] inflammation,[8] fibrosis,[9] HIV,[10] myeloid neoplasms,[11] and cardiovascular disease.[12,13] Therefore, BET proteins are interesting targets for disease treatment.

The BET family comprises bromodomain-containing protein 2 (BRD2), bromodomain-containing protein 3 (BRD3), bromodomain-containing protein 4 (BRD4), and testis-specific bromodomain-containing protein (BRDT). Each BET member is characterized by tandem bromodomains within the N-terminus (normally named bromodomain 1 [BD1] and BD2), an extra-terminal domain (labeled ET), and a variable domain within the C-terminus (Figure 1A). These two bromodomains are conserved in the BET family and between BD1 and BD2. The active site of the bromodomain (also known as the acetylated lysine-binding pocket) recognizes the acetylated lysine of histone tails.[14] However, the two individual bromodomains of the BET family have distinct functions.[15−20] BD1 plays an important role in anchoring proteins to chromatin to maintain basal gene expression.[21,22] In contrast, BD2 binds to acetylated proteins to facilitate gene expression.[22,23] This suggests that selective

Received: June 4, 2023
Accepted: August 25, 2023
Published: September 6, 2023

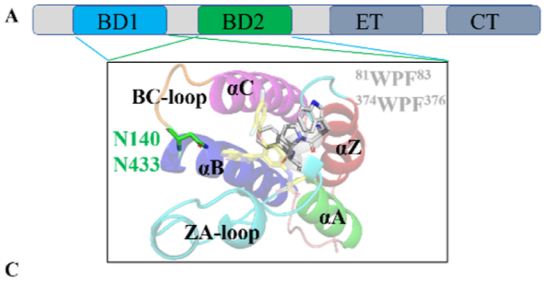

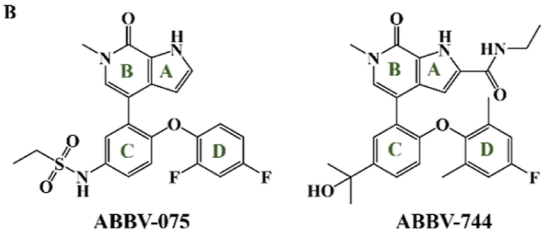

C

IC_{50} (nM)	BRD2-BD1	BRD2-BD2	Fold BD1/BD2	BRD3-BD1	BRD3-BD2	Fold BD1/BD2
ABBV-075	27	7	3.86	15	5	3.00
ABBV-744	2449	8	306.13	7501	13	577.00
IC_{50} (nM)	BRD4-BD1	BRD4-BD2	Fold BD1/BD2	BRDT-BD1	BRDT-BD2	Fold BD1/BD2
ABBV-075	11	3	3.67	36	18	2.00
ABBV-744	2006	4	501.50	1835	19	96.58

D

IC_{50} (nM)	BRD4-BD1	BRD4-BD2	Fold BD1/BD2
ABBV-075	0.55	0.22	0.12
ABBV-744	210.30	0.26	808.85

Figure 1. Structure and biochemical activity for the BET of ABBV-744 and ABBV-075, respectively. (A) Structure of bromodomain-containing protein 4 (BRD4) showing the active site containing bromodomain 1 or 2 (BD1 or BD2). (B) Structure of the pan-BD inhibitor ABBV-075 and pan-BD2 inhibitor ABBV-744. (C) Biochemical activity of ABBV-075 and ABBV-744 targeting BD1 and BD2 toward BET proteins. The selectivity fold for each BD1/BD2 pair is indicated. The biochemical activity was obtained from time-resolved fluorescence energy transfer (TR-FRET) data in Faivre et al.[18] (D) Biochemical activity of ABBV-075 and ABBV-744 targeting BD1 and BD2 of BRD4 from the present study.

targeting of BD1 or BD2 may differentially modify disease activities.

Several small-molecule BET inhibitors were developed for early clinical development or in preclinical studies.[24−30] High efficacy and positive results were found for BET inhibitor treatment of hematological malignancies,[31−34] such as ovarian cancer,[35] metastatic prostate cancer,[36] breast cancer,[37] and small-cell lung cancer.[38] However, some probes designed as early tools exhibited weak and poorly selective binding; thus, it was necessary to develop novel well-characterized probes to ascertain the function of bromodomain family members.[39−45] In addition, some pan-BD inhibitors (defined as having similar inhibitory activity for BD1 and BD2 of BET proteins including the eight bromodomains) have potential applications for academic research or drug development, such as JQ1,[46] I-BET151,[47] ZEN-3694,[48−50] OTX-015,[51,52] NHWD-870,[53] and ABBV-075[54] (Figure S1). However, there are no approved BET inhibitors for therapy as BET inhibition has side effects (for example, thrombocytopenia, anemia, neutropenia, nausea, diarrhea, pneumonia, elevated bilirubin, and fatigue).[55,56] Notably, these safety signals are pharmacology-driven and dose-limiting, preventing BET inhibitors from achieving their full potential owing to limited target engagement at their maximum tolerated dose. Pan-BD1 or pan-BD2 inhibitors show better tolerance than pan-BD inhibitors and have reduced side effects.[18,19] Nevertheless, the high sequence homology and structural similarity between the BD domains among BET family members have limited the development of selective BD inhibitors.[24,26,43,57,58] Thus, selective BD inhibitors are urgently required for disease treatment.

Pan-BD1 inhibitors (which have higher inhibitory activity for BD1 than BD2 of BET proteins) are comparable to pan-BD inhibitors, such as MS436,[59] Olinone,[60] MS402,[61] 3U,[62] GSK778,[19] ZL0516,[63] UMN627,[64] and GSK789.[65] In turn, pan-BD2 inhibitors (which have higher inhibitory activity for BD2 than BD1 of BET family members) are mostly effective for their anti-inflammatory properties; for example, RVX-208,[66] GSK340,[67] BY27,[68] ABBV-744,[69] GSK046,[19] SJ432,[70] GSK097,[71] GSK549,[71] GSK737,[72] and CDD-1102.[73] There are more than 700 published complex crystal structures for BET proteins in the RCSB Protein Data Bank (PDB)[74−76] that help understand selectivity mechanisms. However, the details of the molecular-specific core must be further studied at the atomic level. This study selected the pan-BD inhibitor (ABBV-075) and pan-BD2 inhibitor (ABBV-744) (Figure 1B) to study the selectivity mechanism of the pyrrolopyridone core compounds between BRD4-BD1 and BRD4-BD2.

ABBV-075 (*N*-[4-(2,4-difluorophenoxy)-3-(6-methyl-7-oxo-1*H*-pyrrolo[2,3-*c*]pyridin-4-yl)phenyl]ethanesulfonamide, Mivebresib, CAS NO. 1445993-26-9) is a pan-BD inhibitor used to treat multiple myeloma, acute myeloid leukemia, and solid tumors.[54,77] Clinical trials of ABBV-075 were performed for myelofibrosis (NCT04480086) and cancer (NCT02391480). However, ABBV-075 caused adverse events such as fatigue, thrombocytopenia, dysgeusia, anemia, gastrointestinal bleeding, hypertension, decreased appetite, aspartate aminotransferase elevation, and nausea in certain patients with solid tumors (uveal melanoma and colorectal, pancreatic, breast, head, and neck cancer).[78] ABBV-075 binds to the acetylated lysine site of BET and inhibits BET protein functions.[54] ABBV-075 inhibits BET activity in vitro, with half maximal inhibitory concentration (IC_{50}) values in the nanomolar range (27, 7, 15, 5, 11, 3, 36, and 18 nM for BRD2-BD1, BRD2-BD2, BRD3-BD1, BRD3-BD2, BRD4-BD1, BRD4-BD2, BRDT-BD1, and BRDT-BD2, respectively), as shown in Figure 1C.[18] In contrast, ABBV-744 is a pan-BD2 inhibitor that mainly inhibits the function of BD2 with IC_{50} values of 2449, 8, 7501, 13, 2006, 4, 1835, and 19 nM for BRD2-BD1, BRD2-BD2, BRD3-BD1, BRD3-BD2, BRD4-BD1, BRD4-BD2, BRDT-BD1, and BRDT-BD2, respectively.[18] ABBV-744 (*N*-ethyl-4-[2-(4-fluoro-2,6-dimethylphenoxy)-5-(2-hydroxypropan-2-yl)phenyl]-6-methyl-7-oxo-1*H*-pyrrolo[2,3-*c*]pyridine-2-carboxamide, CAS NO. 2138861-99-9) was evaluated in clinical trials (NCT03360006 and NCT04454658). The crystal structures of inhibitor−protein complexes are published for ABBV-075/BRD4-BD1 (PDB entry: 5UVW[79]), ABBV-744/BRD2-BD1

https://doi.org/10.1021/acsomega.3c03935
ACS Omega 2023, 8, 33658−33674

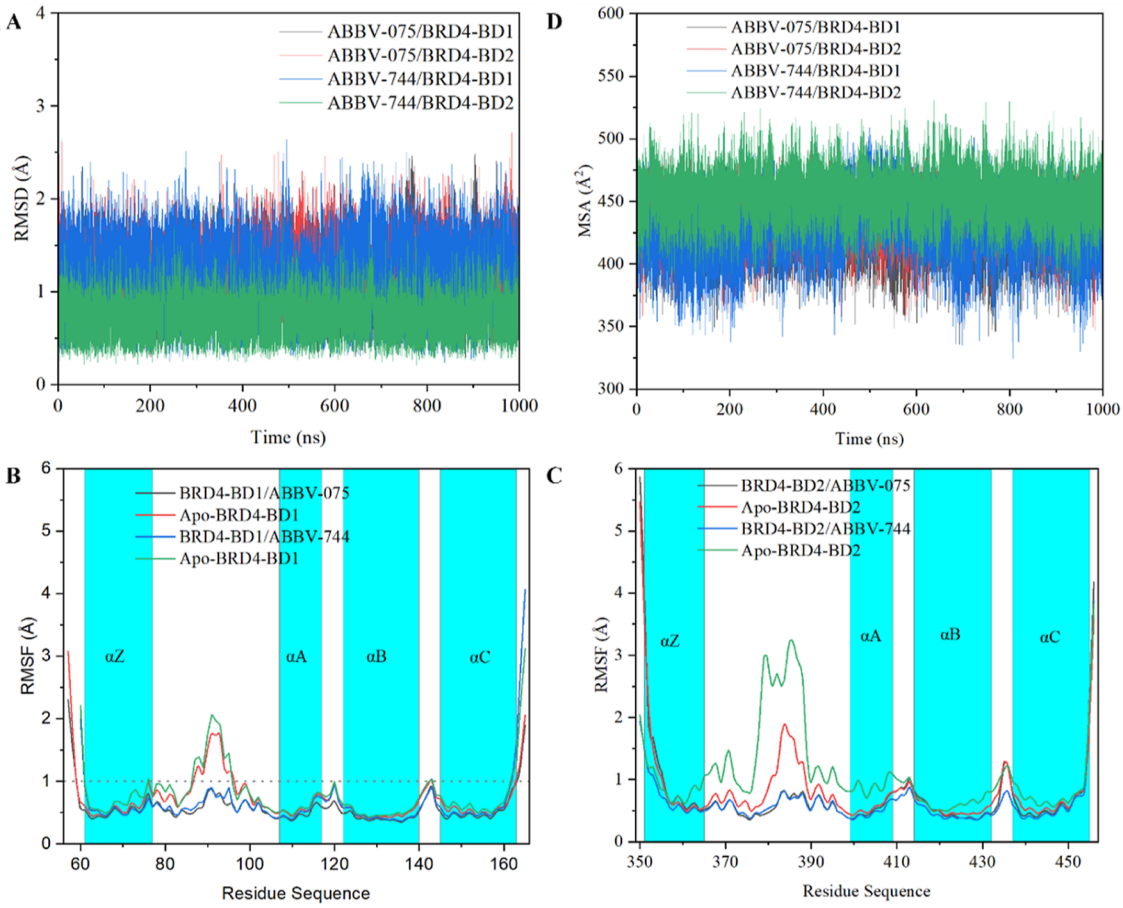

Figure 2. System stability for inhibitor/BRD4 complex systems. (A) rmsd value of heavy backbone atoms for proteins (BRD4-BD1 or BRD4-BD2) along the 1000 ns MD simulation for ABBV-075/BRD4 and ABBV-744/BRD4 systems. RMSF variations for the Cα atom of BRD4-BD1 (B) and BRD4-BD1 (C) of ABBV-075/BRD4 and ABBV-744/BRD4 systems from the 1000 ns MD simulation. (D) Interface of the MSA for ABBV-075/BRD4 and ABBV-744/BRD4 systems.

(6ONY[18]), and ABBV-744/BRD2-BD2 (6E6J[18]). The present study constructed ABBV-075/BRD4-BD2, ABBV-744/BRD4-BD1, and ABBV-744/BRD4-BD2 complex structures to study the selectivity mechanism of pyrrolopyridone core compounds.

A reliable inhibitor−protein complex structure plays a vital role in drug development.[80−82] Computational methods, such as homology modeling,[83−85] molecular docking,[86−88] molecular dynamics (MD) simulation,[89−91] binding free energy calculation,[92−94] and others[95−97] are widely employed. These methods were used to elucidate the binding models and mechanisms of inhibitor/BET systems.[98−107] Thus, MD simulations and binding free energy calculations were employed in the present study to elucidate the selective-BD2 mechanism for the pyrrolopyridone core compounds.

In this study, the binding models of pyrrolopyridone analogues were obtained from MD simulations for a selective-BD2 inhibitor (ABBV-744) and pan-BD inhibitor (ABBV-075). Additionally, binding free energy calculations were employed to quantify binding affinity, and the contribution of every residue also was obtained from energy decomposition using the molecular mechanics/generalized Born and surface area continuum solvation (MM/GBSA) method. The selective-BD2 mechanism of pyrrolopyridone analogues was constructed at the atomic level from MD simulation and binding free energy calculations. We believe that the selective-BD2 mechanism of pyrrolopyridone analogues may provide valuable information to design highly selective-BD2 inhibitors.

2. RESULTS AND DISCUSSION

2.1. System Stability. The initial complex structures for ABBV-075 or ABBV-744 binding to BRD4-BD1 or BRD4-BD2 were constructed based on their crystal structures (Figure S2). The conformations of ABBV-075 and ABBV-744 obtained from their crystal structures were selected as the initial conformations for MD simulations (Figure S3). Although this may not be the best conformation for complex formation, it was the best for use as the initial model. The root mean square deviation (rmsd) of the backbone atoms in proteins (BRD4-BD1 or BRD4-BD2) and of the heavy atoms of the ligands (ABBV-075 or ABBV-744) were calculated after superposition with the initial coordinates to consider the conformational changes of BRD4 and the inhibitors (Figures 2A, S4, and S5). The vibration range of the rmsd value of BRD4 was lower than that of the ligand molecule with the exception of the ABBV-744/BRD4-BD2 system (Figure S4). The rmsd values of ABBV-075/BRD4-BD1, ABBV-075/BRD4-BD2, ABBV-744/BRD4-BD1, and ABBV-744/BRD4-BD2 were 0.79 ± 0.14, 1.37 ± 0.38, 1.06 ± 0.29, and 1.09 ± 0.20 Å, respectively, for the first replicate simulation (Table S1). The rmsd values for the heavy atoms of ABBV-075 and ABBV-744 were higher than those of BRD4-BD1 and lower than those of BRD4-BD2.

https://doi.org/10.1021/acsomega.3c03935
ACS Omega 2023, 8, 33658−33674

System	Acceptor	Donor	Occupancy (%)		
			1	2	3
ABBV-075/BRD4-BD1	8NG@O1	N140@ND2	99.65	99.58	99.66
	N140@OD1	8NG@N1	97.43	97.45	97.25
	8NG@O3	D88@N	97.18	98.91	89.61
ABBV-075/BRD4-BD2	8NG@O1	N433@ND2	99.69	99.70	99.74
	N433@OD1	8NG@N1	92.46	93.47	93.55
	8NG@O3	D381@N	99.45	99.76	99.77
ABBV-744/BRD4-BD1	HWV@O2	N140@ND2	95.72	99.22	99.13
	N140@OD1	HWV@N3	95.99	95.69	95.18
	HWV@O4	D88@N	67.95	70.44	73.51
	N140@OD1	HWV@N2	97.14	96.91	96.67
ABBV-744/BRD4-BD2	HWV@O2	N433@ND2	99.60	99.67	99.60
	N433@OD1	HWV@N3	99.48	99.46	99.54
	HWV@O4	D381@N	78.01	78.14	77.04
	N433@OD1	HWV@N2	99.71	99.69	99.68

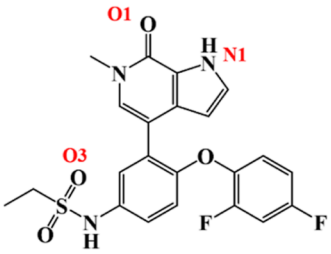

ABBV-075: 8NG

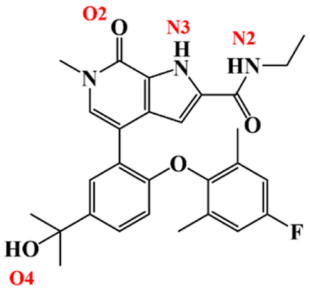

ABBV-744: HWV

Figure 3. Hydrogen bond analysis between pyridine inhibitors and BRD4. The occupancy was expressed as a percentage of the period (1000 ns, 100,000 frames) during which specific hydrogen bonds were formed. The hydrogen bond was confirmed when the distance between the acceptor and donor atoms < 3.5 Å, with an internal angle between the H-acceptor and H-donor > 120°.

However, some regions of the protein fluctuated far from the stable baseline (Figure S5), such as 800−1000 ns of replicate 2 for ABBV-075/BRD4-BD1 (Figure S6), 730−740 ns of replicate 3 for ABBV-075/BRD4-BD2 (Figure S7), and 600−800 ns of replicate 1 for ABBV-744/BRD4-BD1 (Figure S8). Other fluctuating regions were checked from the frames extracted from the regions shown in Figures S9−S16. These results indicated that the small compounds were bound in the binding site of the BD1 or BD2 domain. The maximum rmsd values were 2.03, 2.69, 2.74, and 1.93 Å for replicate 1 of ABBV-075/BRD4-BD1, ABBV-075/BRD-BD2, ABBV-744/BRD4-BD1, and ABBV-744/BRD4-BD2, respectively. The maximum rmsd value for the 12 complex systems was 2.74 Å from replicate 1 for ABBV-744/BRD4-BD1. This suggested that BRD4 was stable in the simulations. In addition, the ligand molecule had a maximum rmsd value of 2.77 Å using replicate 3 for ABBV-744/BRD4-BD1. This showed that ABBV-075 and ABBV-744 were stably bound in the active site of BRD4-BD1 or BRD4-BD2. Thus, the 12 complex systems were stable and were used in subsequent analyses.

The root mean square fluctuations (RMSFs) for BRD4-BD1 and BRD4-BD2 were analyzed with the backbone heavy atoms based on 1000 ns MD simulations (Figure 2B,C). The BRD4-BD1 and BRD4-BD2 systems without ABBV-075 and ABBV-744 inhibitors (named Apo-BRD4-BD1 and Apo-BRD4-BD2) were also analyzed as reference systems. Interestingly, the fluctuation in BRD4-BD1 and BRD4-BD2 increased from inhibitor binding to unbinding (Figures S17 and S18). In particular, the ZA-loop is more flexible for apo-BRD4 than for ABBV-075 or ABBV-744 binding to the active sites of BRD4-BD1 or BRD4-BD2 region; this ZA-loop plays an important role in inhibitor binding.[108−113] Thus, the stability of the active sites of BRD4-BD1 and BRD4-BD2 could be increased by inhibitor binding. In addition, both the N-terminal and C-terminal regions showed larger fluctuations than those of the other regions in the eight systems. The αZ, αA, αB, and αC domains were more stable than the ZA-loop, AB-loop, and BC-loop for the four complex systems excluding the N- and C-terminal regions. Furthermore, the overall structures of BRD4-BD1 and BRD4-BD2 were stable in the simulation.

The molecular surface area (MSA) was used to determine the flexibility of BRD4-BD1 or BRD4-BD2 with ABBV-075 or ABBV-744 binding to the acetylated lysine-binding pocket (Figures S19−S22). The MSA of the inhibitor/BRD4 complex [MSA(complex)], BRD4 [MSA(receptor)], and inhibitor [MSA(ligand)] were estimated using linear combinations of the pairwise overlap algorithm.[114] The interface between the ligand and protein was calculated as MSA(interface) = [(MSA(receptor) + MSA(ligand) − MSA(complex)]/2 (Figure 2D). The MSA(interface) of the ABBV-075/BRD4-BD1, ABBV-075/BRD4-BD2, ABBV-744/BRD4-BD1, and ABBV-744/BRD4-BD2 complexes (replicate 2) were 427.17 ± 16.63, 436.47 ± 15.68, 428.44 ± 19.42, and 443.82 ± 116.17 Å^2, respectively. This suggests that the MSA(interface) was larger for BRD4-BD2 than for BRD4-BD1 (Table S2). Therefore, the greater structural flexibility of BRD4-BD2 results from the larger MSAs of the inhibitor/BRD4-BD2 than those of the inhibitor/BRD4-BD1. This certainly considerably affects the binding of pyrrolopyridone analogues with BRD4-BD1 and BRD4-BD2.

Snapshots were drawn and extracted from the MD simulations at 100, 200, 300, 400, 500, 600, 700, 800, 900, and 1000 ns to demonstrate the conformational change following ABBV-075 or ABBV-744 binding to BRD4-BD1 or BRD4-BD2 (Figures S23−S34). ABBV-075 and ABBV-744 remained stable upon binding with BRD4-BD1 and BRD4-BD2; this agrees with the rmsd and RMSF analyses. These stable binding models indicate that both ABBV-075 and ABBV-744 can bind to the acetylated lysine sites of BRD4.

The main binding conformation of the inhibitor to BRD4 was obtained from cluster analysis based on the average linkage cluster algorithm. The representative frames (centroid frame of

https://doi.org/10.1021/acsomega.3c03935
ACS Omega 2023, 8, 33658−33674

Table 1. van der Waals Interactions (E_{vdW}), Decomposition and Electrostatic Interactions (E_{ele}), Solvation Free Energies (E_{polar}), Nonpolar Solvation Energies ($E_{nonpolar}$), Entropy (TS_{total}), and Binding Free Energies (G^{cal}_{bind}) of the Inhibitor/BRD4 Systems

energy (kcal/mol)	ABBV-075		ABBV-744	
	BRD4-BD1	BRD4-BD2	BRD4-BD1	BRD4-BD2
ΔE_{vdW}	−44.89 ± 0.32[a]	−45.34 ± 0.43	−46.39 ± 0.16	−48.94 ± 0.56
ΔE_{ele}	−27.81 ± 1.98	−21.18 ± 0.59	−22.51 ± 0.73	−23.66 ± 0.06
ΔE_{polar}	44.78 ± 1.35	36.67 ± 0.47	32.12 ± 0.41	30.27 ± 0.06
$\Delta E_{nonpolar}$	−6.12 ± 0.04	−6.30 ± 0.02	−6.14 ± 0.07	−6.54 ± 0.04
ΔE_{gas}	−72.70 ± 2.22	−66.52 ± 0.87	−68.92 ± 0.62	−72.60 ± 0.52
ΔE_{solv}	38.65 ± 1.31	30.37 ± 0.45	25.98 ± 0.43	23.73 ± 0.02
Δ(*E*gas + *E*sol)	−34.05 ± 0.91	−36.15 ± 0.48	−42.94 ± 0.20	−48.87 ± 0.50
ΔTS_{total}	−25.56 ± 1.22	−24.14 ± 0.06	−26.20 ± 0.76	−26.30 ± 0.97
ΔG^{cal}_{bind}	−8.49 ± 2.11	−12.01 ± 0.51	−16.75 ± 0.73	−22.56 ± 0.52

[a]Average ± standard deviation.

the highest-occupancy cluster) for ABBV-075 or ABBV-744 binding to BRD4 systems were obtained from cluster analysis (Detailed information for cluster analysis can be found in the Supporting Information). There was only one cluster, excluding ABBV-075/BRD4-BD1 (replicate 2, Figure S35) and ABBV-075/BRD4-BD2 (Figures S36−S38 for replicate 1, 2, and 3), based on epsilon = 2.0 Å. The rmsd values among the centroid frame of the first cluster for ligand/BRD4 complex system simulations were under 0.60, 1.45, 0.66, and 0.89 Å among the three replicate simulations for ABBV-075/BRD4-BD1, ABBV-075/BRD4-BD2, ABBV-744/BRD4-BD1, and ABBV-744/BRD4-BD2, respectively (Figure S39). In addition, the rmsd values between BRD4-BD1 and BRD4-BD2 were over 1.33 and 1.25 Å for ABBV-075/BRD4 and ABBV-744/BRD4, respectively. The rmsd values suggested that ABBV-075/BRD4-BD2 showed more fluctuations than those of the other three complex systems.

2.2. Hydrogen Bond Analysis. Hydrogen bonds formed between small chemical scaffolds of BET inhibitors and N140 (N433) of the acetylated lysine site of BRD4-BD1 (BRD4-BD2) are commonly required for binding of BET inhibitors.[99,115−120] Hydrogen bonding plays an important role in drug design.[121−124] In particular, it plays a significant role in competitive inhibitor binding to the active site of the bromodomain of BET proteins, including BRD4-BD1 and BRD4-BD2 (Figure 3). In this study, the hydrogen bond was confirmed when the distance between the acceptor and donor atoms was less than 3.5 Å, and the internal angle of the acceptor···H-donor was above 120°. The hydrogen bond numbers (i.e., the statistical hydrogen bond count along the 1000 ns MD simulation with 100,000 frames) for ABBV-075 or ABBV-744 binding to BRD4-BD1 or BRD4-BD2 were examined from the simulation trajectory (Figures S40). The ABBV-075/BRD4-BD2 system had hydrogen bond numbers (3.06, 3.08, and 3.08 for replicate 1, 2, and 3, respectively) similar to those of the ABBV-075/BRD4-BD1 system (3.31, 3.36, and 3.28 for replicate 1, 2, and 3, respectively). However, the hydrogen bond number of ABBV-075/BRD4 (≤3.36) was less than that of the ABBV-744/BRD4 system (≥4.14, Table S3). The frame count for the number of hydrogen bonds was subjected to statistical analysis (Figure S41). There were approximately three hydrogen bonds that occupied over 60 and 80% of the simulation time for ABBV-075/BRD4-BD1 and ABBV-075/BRD4-BD2, respectively. Simultaneously, the hydrogen bond numbers of the ABBV-744/BRD4 system (mostly located at 3−5) were more widely distributed than those of the ABBV-075/BRD4 system. This indicates that ABBV-744 forms more hydrogen bonds with BRD4 than ABBV-075.

Additionally, occupancy analysis of the hydrogen bonds was performed for the 12 inhibitor/BRD4 systems. Three hydrogen bonds with high occupancies (≥90%) were found for ABBV-075 (defined as 8NG) binding with BRD4-BD1 or BRD4-BD2 (Figure 3). The occupancies of hydrogen bonding between the O1 of ABBV-075 (defined as 8NG) and the ND2 atom of N140 were 99.65, 99.58, and 99.66% for replicates 1, 2, and 3 of the ABBV-075/BRD4-BD1 systems, respectively. N140 (OD1) also formed a hydrogen bond with the N1 atom of ABBV-075 with 97.00% occupancy. The same site residue N433 of BRD4-BD2 also formed two hydrogen bonds with ABBV-075 with over 92.00% occupancy. Thus, hydrogen bonds formed between the 6-methyl-1,6-dihydro-7*H*-pyrrolo-[2,3-*c*]pyridin-7-one group of ABBV-075 and N140 or N433 were used to locate the core acetylated lysine site of BRD4-BD1 or BRD4-BD2. These two hydrogen bonds were also found during ABBV-744 (named HWV) binding with BRD4 (hydrogen bond between the N3 or O2 of ABBV-744 with N140 or N433 of BRD4), such as the N3 of ABBV-744 formed with the OD1 atom of N140 with occupancies ≥ 95.00% in the 1000 ns simulation time. Therefore, the N140 and N433 key residues do not contribute to selectivity but play an important role in binding activity. Moreover, the hydrogen bonds between the side chains of ABBV-075 (ethanesulfonamide group) and D88 (or D361) were more stable (≥97.00%) than those between the propan-2-ol groups of ABBV-744 and D88 (67.95−73.51%) or D361 (77.04−78.14%). D88 and D361 may contribute to inhibitor binding. In contrast, N2 of ABBV-744 formed stable hydrogen bonds with BRD4, with occupancies of over 96.00% for ABBV-744/BRD4-BD1 systems and over 99.00% for ABBV-744/BRD4-BD2 systems. However, this hydrogen bond was not observed in the binding of ABBV-075 to BRD4. Thus, the hydrogen bond between the N140 (or N433) residue and the N2 atom of ABBV-744 plays an important role in its binding to BRD4. This agrees with experimental and theoretical results.[18,69]

Moreover, the distances between the acceptor and donor atoms and the angles among acceptor, hydrogen, and donor atoms were calculated with the 12 complex systems in 1000 ns simulations (Figures S42−S53). The hydrogen bonds between the pyrrolopyridone core groups of ABBV-075 (or ABBV-744) and N140 (or N433) of BRD4 were stable at most simulation times. However, the fluctuation regions showed unstable

https://doi.org/10.1021/acsomega.3c03935
ACS Omega 2023, 8, 33658−33674

hydrogen bonds, such as hydrogen bonds (D88_N-8NG_O3) at 750−780 ns for the ABBV-075/BRD4-BD1 replicate 1 (ABBV-075/BRD4-BD1_1) system, wherein oxygen atom O3 was far from the N atom of N140 (Figure S54). The distance of D88@N_8NG@O3 for ABBV-075/BRD4-BD1_1, ABBV-075/BRD4-BD1_2, and ABBV-075/BRD4-BD1_3 was 3.08 ± 0.48, 2.97 ± 0.19, and 3.14 ± 0.59 Å, respectively (Table S4). The similar hydrogen bond of ABBV-075/BRD4-BD2 (D381@N-8NG@O3) had a comparable strength from a closed distance (2.91 ± 0.21, 2.90 ± 0.13, and 2.90 ± 0.13 Å for replicate 1, 2, and 3, respectively). However, this hydrogen bond for ABBV-744/BRD4, whose distance was greater than 3.50 Å, was weaker than that for ABBV-075/BRD4. In contrast, N140@OD1_HWV@N2 and N433@OD1_HWV@N2 could compensate for the binding affinity. Hydrogen bonds were employed to locate the conformation of ABBV-075 or ABBV-744 binding to the acetylated lysine site and to increase binding affinity.

2.3. Binding Free Energies. The binding information for ABBV-075 or ABBV-744 with BRD4 was obtained from MD simulations. However, the binding affinity for pyrrolopyridone analogues could not be obtained. Therefore, the binding affinity for inhibitor binding with BRD4 was calculated using the MM/GBSA method from the last 100 ns of the simulation for every complex system. The calculated binding free energies for ABBV-075 or ABBV-744 binding with BRD4 are shown in Tables 1 and S5−S17. The triplicate inhibitor bindings with the BRD4 systems were considered in this study and showed similar free energy binding, such as −17.58, −16.46, and −16.20 kcal/mol for three replicate simulations of the ABBV-744/BRD4-BD1 system. Thus, the average binding free energy from three replicate simulations was selected to discuss the four binding models. The two inhibitors bound to the acetylated lysine site of BRD4 with binding energies of −8.49, −12.01, −16.75, and −22.56 kcal/mol for ABBV-075/BRD4-BD1, ABBV-075/BRD4-BD2, ABBV-744/BRD4-BD1, and ABBV-744/BRD4-BD2, respectively. ABBV-744 showed lower free energy while binding to BRD4-BD2 than that evinced by ABBV-075. In addition, the inhibition activity of ABBV-075 and ABBV-744 for BRD4-BD1 and BRD4-BD2 was tested at Shanghai ChemPartner Co., Ltd., and the results revealed IC_{50} values of 0.55, 0.22, 210.30, and 0.26 nM for ABBV-075/BRD4-BD1, ABBV-075/BRD4-BD2, ABBV-744/BRD4-BD1, and ABBV-744/BRD4-BD2, respectively (Figures 1D and S55). Detailed information on the homogeneous time-resolved fluorescence (HTRF) assay is provided in the Supporting Information. The selectivity of ABBV-744 was verified using binding free energy calculations and HTRF assays.

The entropy and enthalpy values for ABBV-075 binding with BRD4-BD1 were −25.56 and −34.05 kcal/mol, respectively. In comparison, ABBV-075 binding with BRD4-BD2 showed values of −24.14 and −36.15 kcal/mol for entropy and enthalpy, respectively. The negative entropy and enthalpy indicated that ABBV-075 binding to BRD4-BD1 and BRD4-BD2 is an enthalpy-driven process. The entropy values for ABBV-744 binding with BRD4-BD1 and BRD4-BD2 were −26.20 and −26.30 kcal/mol, respectively. The enthalpy values for ABBV-744/BRD4-BD1 and ABBV-744/BRD4-BD2 were −42.94 and −48.87 kcal/mol, respectively. However, the entropy values for inhibitor binding with BRD4-BD1 or BRD4-BD2 did not significantly differ (for example, −25.56 and −24.14 kcal/mol for ABBV-075 binding with BD1 and BD2, respectively). This suggests that entropy does not affect the binding free energy between BD1 and BD2. However, the enthalpy differences between BD1 and BD2 domains were 2.10 and 5.92 kcal/mol for ABBV-075 and ABBV-744, respectively. Thus, the difference in inhibitor binding to BRD4-BD1 and BRD4-BD2 is enthalpy-driven. The entropy differences between ABBV-075 and ABBV-744 were 0.64 and 2.16 kcal/mol for BRD4-BD1 and BRD4-BD2, respectively, whereas enthalpy differences between ABBV-075 and ABBV-744 were 8.90 and 12.72 kcal/mol for BRD4-BD1 and BRD4-BD2, respectively. Therefore, enthalpy may affect the selectivity for pyrrolopyridone BD2-selective inhibitors.

The van der Waals (vdW) interactions (ΔE_{vdW}) between ABBV-075 and BRD4 were −44.89 and −45.34 kcal/mol for BRD4-BD1 and BRD4-BD2, respectively (Figure S56). This suggests that vdW interactions mainly contribute to ABBV-075 binding to BRD4. The ΔE_{ele} was −27.81 and −21.18 kcal/mol for ABBV-075/BRD4-BD1 and ABBV-075/BRD4-BD2, respectively. Additionally, electrostatic interactions were positive for the ABBV-075/BRD4 complex. Alternatively, the vdW interactions for ABBV-744/BRD4-BD1 and ABBV-744/BRD4-BD2 were −46.39 and −48.94 kcal/mol, respectively. The electrostatic interaction was over −22.51 kcal/mol for the ABBV-744/BRD4 systems. The vdW interactions mainly contributed to the binding of ABBV-075 and ABBV-744 to BRD4.

The binding interaction force between small inhibitors and their targets is usually divided into two major factors: the polar term ($E_{ele} + E_{polar}$) and nonpolar term ($E_{vdW} + E_{nonpolar}$). The polar terms exhibited positive values when the inhibitor was bound to BRD4. For example, the polar term values were 16.97, 15.49, 9.61, and 6.61 kcal/mol for ABBV-075/BRD4-BD1, ABBV-075/BRD4-BD2, ABBV-744/BRD4-BD1, and ABBV-744/BRD4-BD2, respectively. This suggests that polar interactions are negative during ABBV-075 and ABBV-744 binding with BRD4. In contrast, the nonpolar terms contributed −51.02 kcal/mol for ABBV-075/BRD4-BD1, −51.63 kcal/mol for ABBV-075/BRD4-BD2, −52.54 kcal/mol for ABBV-744/BRD4-BD1, and −55.47 kcal/mol for ABBV-744/BRD4-BD2. The strongly negative values of the nonpolar terms (over −51.00 kcal/mol) suggest that ABBV-075 and ABBV-744 binding to the acetylated lysine site of BRD4 is mainly due to the nonpolar terms. In other words, the polar term was unfavorable for the binding of ABBV-075 and ABBV-744 to BRD4-BD1 and BRD4-BD2. Conversely, the nonpolar term was favorable for the binding of these two inhibitors.

2.4. Free Energy Decomposition. The binding free energy for complex systems was similar among the three replicate simulations. For example, ABBV-744/BRD4-BD1 complex systems showed −17.58, −16.46, and −16.20 kcal/mol values for the three replicates, whereas ABBV-744/BRD4-BD2 complex systems showed −22.61, −22.02, and −22.56 kcal/mol values for the three replicates. Thus, only the first simulation of the four complex systems was selected to perform energy decomposition in this study. The MM/GBSA method was used to estimate interaction energies per residue. The key residues were defined as those contributing over 1 kcal/mol energy to inhibitor binding with BRD4 in any complex (Tables S18−S21).

Residues P82, F83, V87, D88, L92, L94, N140, and I146 contributed > 1 kcal/mol to the formation of a stable complex in the ABBV-075/BRD4-BD1 system (Figure 4). N140

https://doi.org/10.1021/acsomega.3c03935
ACS Omega 2023, 8, 33658−33674

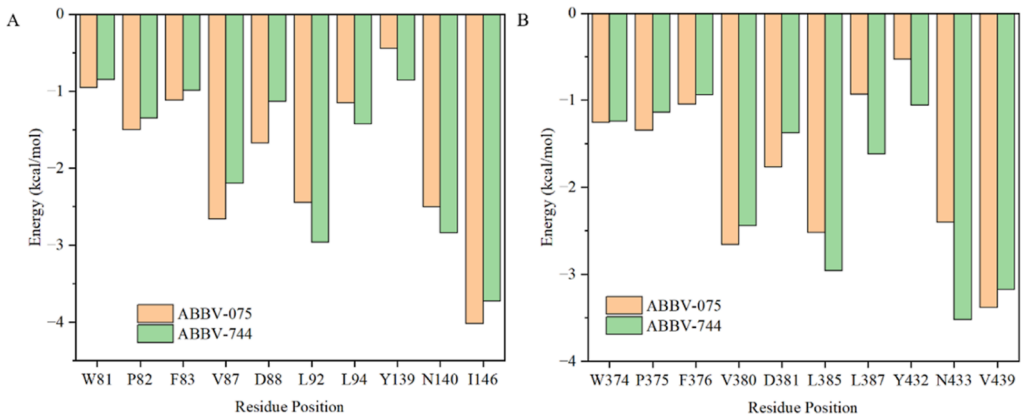

Figure 4. Decomposition energy for inhibitor binding with bromodomain-containing protein 4 (BRD4)-bromodomain 1 (BD1) and BRD4-BD2. (A) Partial residues that contributed energy for ABBV-075 and ABBV-744 binding with BRD4-BD1. (B) Partial residues that contributed energy for ABBV-075 and ABBV-744 binding with BRD4-BD2.

contributed −2.50 kcal/mol from the hydrogen bonds formed with ABBV-075. Additionally, D88 formed a hydrogen bond with ABBV-075 and contributed −1.67 kcal/mol to form the complex system. These two key residues were verified using hydrogen bond analysis. V87 formed vdW (−2.36 kcal/mol) and electrostatic (−1.72 kcal/mol) interactions with ABBV-075 and contributed the most energy to the complex system (−2.66 kcal/mol). Moreover, the side chain of V87 was the main part interacting with ABBV-075 (−2.33 kcal/mol), which correlated with the results of distance analysis between ring B of ABBV-075 and the V87 side chain (Figure S57). In turn, L92 and L94 interacted with rings C and A of ABBV-075 via vdW interactions and contributed binding energies of −2.44 and −1.15 kcal/mol, respectively. A distance analysis between ring C and the L92 side chain was conducted to check the vdW interaction of −1.97 kcal/mol (Figure S58). L94 was identified as the other hydrophobic residue that formed a hydrophobic interaction with ring A of ABBV-075, which was verified by the distance between ring A and L94 (Figure S59). The most favorable residue for ABBV-075 binding with BRD4-BD1 was I146; the interaction with rings A, B, and D of ABBV-075 contributed −4.02 kcal/mol, which was mainly derived from vdW interactions (−3.53 kcal/mol) (Figure S60). In particular, a clip was formed between I146, ring B, and V87 and also between I146, ring A, and L94, as analyzed from the calculated angle for the three regions (Figure S61). Additionally, the ^{81}WPF^{83} motif is an important region for BET inhibitor binding to the acetylated lysine site[99,116,118,125,126] that plays a key role in the binding of ABBV-075 to BRD4-BD1. The contributions of W81, P82, and F83 were −0.96, −1.50, and −1.12 kcal/mol to ABBV-075 binding to the active site of BRD4-BD1, respectively. The WPF motif affected the binding affinity between ABBV-075 and BRD4-BD1 via vdW interactions for W81, P82, and F83 at −1.95, −2.82, and −1.09 kcal/mol, respectively. However, the polar solvation term for these three residues played a negative role in ABBV-075 binding, with values at 2.12, 2.61, and 0.37 kcal/mol, owing to solvent exposure (Figure S62). In summary, W81, P82, F83, V87, D88, L92, L94, N140, and I146 were key residues for ABBV-075 binding to BRD4-BD1.

Residues W374, P375, F376, V380, D381, L385, N433, and V439 contributed over 1 kcal/mol to form a stable complex in the ABBV-075/BRD4-BD2 system. N433 and D381 contributed −2.40 and −1.77 kcal/mol from hydrogen bonds formed with ABBV-075, respectively. V380 contributed to the complex system with −2.66 kcal/mol from the side chain (−2.30 kcal/mol). This agreed with the results of the distance analysis between ring B of ABBV-075 and the side chain of V380 (Figure S63). Moreover, L385 (L387) contributed a binding energy of −2.52 kcal/mol (−0.93 kcal/mol), which was mainly obtained from vdW interactions (−2.02 and −0.78 kcal/mol for L385 and L387, respectively) with ring C of ABBV-075 (Figures S64 and S65). The most favorable residue for ABBV-075 binding with BRD4-BD2 was V439 (−3.38 kcal/mol), which mainly contributed to vdW interactions (−2.80 kcal/mol) with rings A, B, and D of ABBV-075 (Figure S66). In particular, the clip was formed among V439, ring B, and V380 (and among V439, ring A, and L387) based on the angle calculation for these three regions (Figure S67). Additionally, the ^{374}WPF^{376} motif contributed binding energies of −1.25, −1.34, and −1.04 kcal/mol for binding of ABBV-075 to the active site of BRD4-BD2. In summary, W374, P375, F376, V380, D381, L385, N433, and V439 were key residues for ABBV-075 binding to BRD4-BD2.

Residues P82, V87, D88, L92, L94, N140, and I146 contributed over 1 kcal/mol to the formation of a stable complex in the ABBV-744/BRD4-BD1 system. N140 and D88 formed hydrogen bonds with ABBV-744 (−2.84 and −1.14 kcal/mol, respectively). V87 contributed −2.20 kcal/mol to the complex system from vdW forces (−2.23 kcal/mol) and electrostatic interactions (−0.58 kcal/mol), which agrees with the results of distance analysis between ring B of ABBV-744 and the V87 side chain (Figure S68). Moreover, L92 and L94 interacted with rings C and A of ABBV-744 and contributed −2.45 and −1.21 kcal/mol, respectively, from vdW interactions (Figure S69). L94 was identified as another hydrophobic residue that formed a hydrophobic interaction with ring A of ABBV-744 (Figure S70). The most favorable residue for ABBV-744/BRD4-BD1 was I146 with −3.73 kcal/mol energy contribution from the interaction with rings A, B, and D of ABBV-744, which was mainly contributed from vdW interactions with −3.41 kcal/mol (Figure S71). In particular, clips (I146, ring B, and V87 and I146, ring A, and L94) were formed to stabilize the conformation of ABBV-744 in the active site (Figure S72). Additionally, the ^{81}WPF^{83} motif played a key role in ABBV-744 binding with BRD4-BD1 (binding energies of −0.85, −1.35, and −0.99 kcal/mol, respectively). In summary, P82, V87, D88, L92, L94, N140,

https://doi.org/10.1021/acsomega.3c03935
ACS Omega 2023, 8, 33658−33674

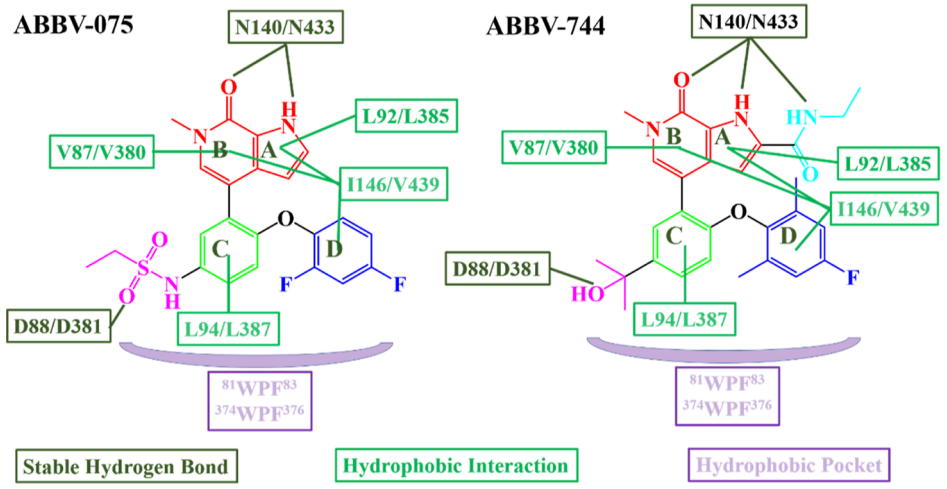

Figure 5. Interaction model of ABBV-075 and ABBV-744 binding with BRD4 obtained from the MD simulations. The key residues involved in hydrogen bonding and hydrophobic interactions are highlighted.

and I146 were key residues for ABBV-744 binding to BRD4-BD1.

Residues W374, P375, F376, V380, D381, L385, N433, and V439 contributed over 1 kcal/mol to form a stable complex in the ABBV-744/BRD4-BD2 system. N433 was the most favorable residue (−3.52 kcal/mol) owing to two hydrogen bonds formed with ABBV-744. Moreover, D381 contributed −1.37 kcal/mol from a hydrogen bond. V380 formed vdW (−2.29 kcal/mol) and electrostatic (−0.75 kcal/mol) interactions with ABBV-075 and contributed −2.44 kcal/mol to the complex system (Figure S73). In turn, L385 and L387 interacted with rings C and A of ABBV-744 via vdW interactions and contributed −2.39 and −1.33 kcal/mol binding energy, respectively (Figure S74). L387 was identified as another hydrophobic residue that formed hydrophobic interactions with ring A of ABBV-744 and contributed −1.61 kcal/mol (Figure S75). V439 interacted with rings A, B, and D of ABBV-744, contributing −3.18 kcal/mol mostly derived from vdW interactions (−2.73 kcal/mol) (Figure S76). In particular, V439 formed a clip with rings B and V380 (and rings A and L387) to retain the conformation of ABBV-744 (Figure S77). Additionally, the ^{374}WPF^{376} motif contributed energies of −1.24, −1.13, and −0.94 kcal/mol to ABBV-744 binding to the active site of BRD4-BD2. In summary, W374, P375, F376, V380, D381, L385, N433, and V439 were key residues for ABBV-744 binding to BRD4-BD2.

2.5. Binding Mechanism. *2.5.1. Binding Model for ABBV-075.* A binding model and key interactions for ABBV-075 binding to BRD4-BD1 were obtained based on MD simulations and binding free energy calculations (Figure 5). The pyrrolopyridone core of ABBV-075 (which was defined as R1) formed a bidentate interaction with N140 or N433. The carbonyl moiety of the pyridone core of ABBV-075 formed a hydrogen bond with the conserved N140 or N433 of BRD4. A contact between N140 or N433 amide carbonyl and the carbonyl moiety of the pyridine core of ABBV-075 was found with lengths of 2.93 ± 0.14 and 2.92 ± 0.14 Å, respectively. The amide group of the pyrrole ring also formed a hydrogen bond with the carbonyl group of N140 or N433. These bidentate hydrogen bonds stabilized the conformation of ABBV-075 and improved its biochemical activity compared to that derived from the N-methyl pyridine, 3-methyl NH-pyridone, and 3-amino-1-methylpyridone groups (Figure S78).[54] Additionally, the pyrrole (ring A) and pyridone rings (ring B) formed hydrophobic interactions with the side chains of V87, L94, and I146 in BRD4-BD1. Rings A and B also formed hydrophobic interactions with V380, L387, and V439 in BRD4-BD2.

The phenyl ring (ring C) of ABBV-075, which was named R2, formed vdW interactions with the side residues L94 or L385. The potency decreased when the nitrogen atom was replaced in the phenyl ring (Figure S79); for example, the pyridine ring with 4.1 ± 0.3 nM (binding affinity K_i) and phenyl ring with 2.4 ± 1.1 nM for BRD4 (BD1 + BD2).[54] The ethanesulfonamide group of ABBV-075 (named R3) reached the pocket via the ZA-loop and was adjacent to the helix of the ZA-loop. Nucleophilic substitution on the central phenyl ring improved the potency compared to that of the unsubstituted phenyl ring because of the hydrogen bond between one of the sulfonamide oxygen atoms and the amide group of D88 or D381. The R3 region maintained the critical position of phenyl ether in the WPF pocket. The ethanesulfonamide chain of ABBV-075 had a similar interaction and potency as pyridone and 2-methylpyrrole-3-carboxamide analogues targeting the BET bromodomain.[127,128] Thus, other groups that incorporate a hydrogen-bond-accepting group can be employed to replace R3, such as amides, sulfones, sulfonamides, and reversed sulfonamides (Figure S80). The phenyl ether region of ABBV-075, which is denoted as R4, interacted with the side residues I146 or V439 mainly through hydrophobic interactions. The binding affinity could be increased by modification with phenyl, pyridyl, pyrimidine, cyclohexyl, or cyclohexane groups. However, replacement using the benzyl 1-methyl-piperidin-4-py aliphatic chain in this region reduced binding affinity.[54] This region is also used to increase the metabolic stability of pyrrolopyridone-based BET inhibitors.[54] A similar trend in binding affinity was observed for substitutions into the R4 region for *N*-methylpyridone and 2-methylpyrrole-3-carboxamide BET inhibitors.[127,128]

ABBV-075 tightly bound to BRD4-BD1 and BRD4-BD2 with K_d = 1.16 and 0.88 nM (isothermal titration calorimetry, ITC), K_d = 14 and 3 nM (surface plasmon resonance, SPR), IC_{50} = 11 and 3 nM (time-resolved fluorescence resonance energy transfer, TF-FRET), and IC_{50} = 34 and 13 nM (NanoBRET), respectively.[18,54] The inhibition activity was also tested using the HTRF assay with IC_{50} = 0.55 and 0.22

https://doi.org/10.1021/acsomega.3c03935
ACS Omega 2023, 8, 33658−33674

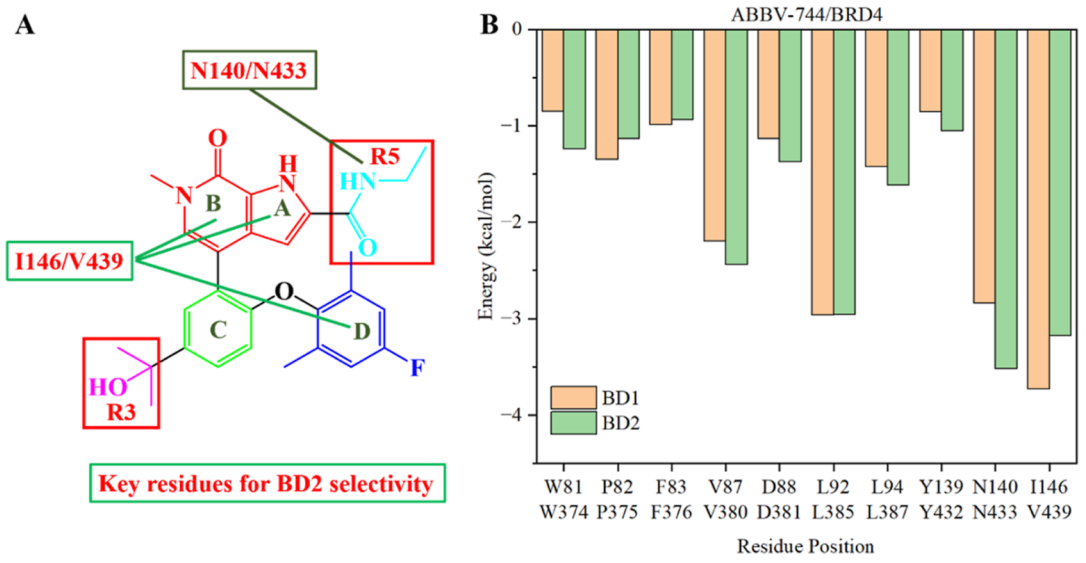

Figure 6. BD2 selectivity mechanism for pyrrolopyridone analogues. (A) Key residues for BD2 selectivity of pyrrolopyridone analogues. (B) Key residues contributing to ABBV-744 binding between BRD4-BD1 and BRD4-BD2.

nM for BRD4-BD1 and BRD4-BD2, respectively. Moreover, average binding energy values of ΔG_{bind}^{cal} = −8.49 and −12.01 kcal/mol were found among three replicate simulations for ABBV-075 binding with BRD4-BD1 and BRD4-BD2, respectively. These results indicate that ABBV-075 is tightly bound to BRD4-BD1 and BRD4-BD2 with only somewhat preferential binding affinity for BRD4-BD2. In addition, the difference in energy between BRD4-BD1 and BRD4-BD2 for the same site residues was below 0.3 kcal/mol (excluding I146 with 0.64 kcal/mol). Thus, W81 (W374), P82 (P375), F83 (F376), V87 (V380), D88 (D381), L92 (L385), L94 (L387), Y139 (Y432), N140 (N433), and I146 (V439) play similar roles in the binding of ABBV-075 to BRD4-BD1 or BRD4-BD2.

2.5.2. Binding Model for ABBV-744. The binding model and key interactions for ABBV-744 binding to BRD4-BD1 and BRD4-BD2 were obtained (Figure 5). The pyrrolopyridone core of ABBV-744 played the same role as that of ABBV-075 in the bidentate hydrogen binding to N140 or N433 (defined as R1). Additionally, the pyrrole ring (ring A) and pyridone ring (ring B) of ABBV-744 formed hydrophobic interactions with the side chains of V87, L94, and I146 in BRD4-BD1, or with V380, L387, and V439 in BRD4-BD2. The phenyl ring (ring C) of ABBV-744 also formed vdW interactions with residues L94 or L385 (named R2). Rings A, B, and C of ABBV-744 were similar to those of ABBV-075 with regard to binding to the active sites of BRD4-BD1 and BRD4-BD2. However, the contribution energy differed; the energy differences between ABBV-075 and ABBV-744 were −0.41 and −1.12 kcal/mol for N140 and N433, respectively. The energy differences between ABBV-075 and ABBV-744 were 0.46, 0.22, −0.52, −0.44, −0.27, −0.68, 0.29, and 0.21 kcal/mol for V87, V380, L92, L385, L94, L387, I146, and V439, respectively. Overall, these residues play an important role in the binding of ABBV-075 or ABBV-744 to BRD4-BD1 or BRD4-BD2.

The methyl carbinol moiety of ABBV-744 was positioned in the cleft adjacent to the ZA-loop, similar to the sulfone of ABBV-075 (named R3). The oxygen atom of the carbinol group as an acceptor atom formed a hydrogen bond with the amino nitrogen atom of D381, and the occupancies in simulation time were 78.01, 78.14, and 77.04% for the three replicate simulations. This hydrogen bond was less stable than that of N433. The dimethyl carbinol moiety (K_i = 1.6 nM) showed a similar binding affinity for BRD4-BD2 as the ethanesulfonamide (K_i = 1.1 nM) and ethyl sulfone (K_i = 1.3 nM) groups. However, these groups showed different binding affinities for BRD4-BD1, such as dimethyl carbinol, ethanesulfonamide, and ethyl sulfone groups with K_i = 520, 49, and 79 nM, respectively (Figure S81).[69] Thus, the R4 region is important for selective targeting of BRD4-BD2. Moreover, the R4 region was employed to improve pharmacokinetic properties.[69] The 4-fluoro-2,6-dimethylphenoxy group of ABBV-744 showed a similar role to that of the 2,4-difluorophenoxy group of ABBV-075, which bound to I146 or V439 of BRD4. This region can be used to reduce the binding affinity of BRD4-BD1 and retain its binding affinity for BRD4-BD2 (Figure S82).[69] This means that the flexibility of the ether linkage needs to be maintained to improve the selectivity of BRD4-BD2 targeting.

The *N*-ethylformamide group of ABBV-744 was defined as R5, which was absent in ABBV-075. The nitrogen atom of the amide group formed hydrogen bonds with N140 or N433, which contributed −2.84 and −3.52 kcal/mol to ABBV-744/BRD4, respectively. The binding affinity without the *N*-ethylformamide group (IC_{50} = 1.3 nM) was similar to that with the *N*-ethylformamide group (IC_{50} = 1.2 nM) for BRD4-BD2. However, the binding affinity for BRD4-BD1 decreased from IC_{50} = 1.8 nM without the *N*-ethylformamide group to IC_{50} = 22 nM with the *N*-ethylformamide group, as shown in Figure S83. Additionally, this region can be used to design dual inhibitors such as those targeting histone deacetylases and BRD4.[129] Thus, the tridentate hydrogen bonds between ABBV-744 (R1 and R5) are important for the binding affinity, especially at the R5 site.

ABBV-744 tightly bound to BRD4-BD2 with K_d = 2 nM (SPR), IC_{50} = 4 nM (TR-FRET), and IC_{50} = 28 nM (NanoBRET).[18] Conversely, ABBV-744 shows weak binding with BRD4-BD1 (K_d = 3300 nM with SPR, IC_{50} = 2006 nM with TR-FRET, and IC_{50} = 21,000 nM with NanoBRET).[18] The inhibition activity of ABBV-744 was also tested using the HTRF assay for BRD4-BD1 and BRD4-BD2 with IC_{50} =

https://doi.org/10.1021/acsomega.3c03935
ACS Omega 2023, 8, 33658−33674

210.30 and 0.26 nM, respectively. Furthermore, the binding free energies for ABBV-744 with BRD4-BD1 and BRD4-BD2 were −16.75 and −22.56 kcal/mol, respectively. These results indicate that ABBV-744 is bound tightly to BRD4-BD2 with greater affinity than to BRD4-BD1. Three pairs of residues had energy differences greater than 0.3 kcal/mol between BRD4-BD1 and BRD4-BD2, such as I146 (V439), N140 (N433), and W81 (W374). Thus, W81 (W374), P82 (P375), V87 (V380), D88 (D381), L94 (L387), Y139 (Y432), N140 (N433), and I146 (V439) play different roles for ABBV-744 binding with BRD4-BD1 or BRD4-BD2.

2.5.3. Selective-BD2 Mechanism. Some residues close to the active site of the bromodomain were different between BRD4-BD1 and BRD4-BD2, including D144/H437 and I146/V439, as determined from the protein sequences of the binding sites of BRD4-BD1 and BRD4-BD2. I146 contributed −4.02 and −3.73 kcal/mol for ABBV-075 and ABBV-744 binding with BRD4-BD1, respectively (Figure 6). I146 had a greater affinity for ABBV-075 than for ABBV-744, with a 0.29 kcal/mol energy difference. Moreover, the energy difference between ABBV-075 and ABBV-744 for V439 was 0.21 kcal/mol, which is similar to that of I146. Thus, the energy contribution of I146/V439 to ABBV-075 and ABBV-744 was relatively small. Alternatively, the energy difference between BRD4-BD1 (I146) and BRD4-BD2 (V439) was 0.64 and 0.55 kcal/mol for ABBV-075 and ABBV-744, respectively. This indicated that I146 and V439 mainly contributed to the difference between BD1 and BD2. The side chain of I146 (isobutyl group) was longer than that of V439 (isopropyl group) in the complex structures. Both I146 and V439 interacted with the pyrrolopyridone core via vdW interactions (Figure S84). Thus, different residues (I146/V439) contribute to selective binding between BRD4-BD1 and BRD4-BD2.

D144 and H437 residues were found to be non-essential for ABBV-075 and ABBV-744 binding to BRD4. This indicated that D144 and H437 cannot contribute to the selectivity between BD1 and BD2 for ABBV-075 and ABBV-744. The energy contribution of D144 was positive with 0.30 and 0.39 kcal/mol for ABBV-075 and ABBV-744, respectively. Moreover, D144 was far from R5 of ABBV-744, which was absent in ABBV-075 (Figure S85). The imidazole ring of H437 was close to that of the *N*-ethylformamide group of ABBV-744. However, the interaction between the imidazole ring of H437 and the *N*-ethylformamide group was weakened (−0.30 and −0.57 kcal/mol for ABBV-075 and ABBV-744, respectively) owing to the *N*-ethylformamide group forming a hydrogen bond with N433. Therefore, the BC-loop (including D144 and H437) can be used to improve the selectivity between BD1 and BD2.

Additionally, D144/H437 contributed to the BD2 selectivity for ABBV-744 as shown by the crystal structure for ABBV-744/BRD2-BD1 (PDB ID: 6ONY[18]) and ABBV-744/BRD2-BD2 (PDB ID: 6E6J[18]). The imidazole of H437 interacts with ring D as shown by the edge−to−face interaction with a distance (defined as the distance between the center of the imidazole ring of H437 and that of ring D of the inhibitors) of 5.27 and 4.88 Å for ABBV-744 and compound 18, respectively (Figure S86). The energy for this edge−to−face interaction was calculated and is shown in Figure S87. The lowest energy was −2.85 kcal/mol with 4.58 Å, which was similar to that of compound 18 binding with BRD4-BD2 (4.88 Å) and lower than that of ABBV-744 binding with BRD2-BD2 (5.27 Å). Moreover, the distances were also calculated for ABBV-744 and ABBV-075 binding with BRD4-BD2 in the simulations (Figure S88). The distances were 6.12 ± 0.53, 5.93 ± 0.53, and 5.92 ± 0.61 Å for replicate 1, 2, and 3 simulations of ABBV-075/BRD4-BD2, respectively. Additionally, the distances of ABBV-744/BRD4-BD2 were 5.93 ± 0.49, 5.30 ± 0.42, and 5.36 ± 0.52 Å, respectively. We speculate that the weaker edge−to−face interaction obtained in the simulation than that in the crystal structures resulted from the solvent environment. However, the edge−to−face interaction plays an important role in ligand binding with proteins.[130−133] Furthermore, the dimethyl phenyl and ethyl amide groups have been applied to increase the selectivity between BRD4-BD1 and BRD4-BD2.[134−136] Thus, this edge−to−face interaction warrants further investigation in future studies.

In addition, the same site residues contributed energy differences between BD1 and BD2, such as W81/W374 with a −0.30 kcal/mol energy difference for ABBV-074 binding with BRD4. The WPF motif is conserved among BRD2, BRD3, BRD4, and BRDT. However, W374 (−1.25 and −1.24 kcal/mol for ABBV-075 and ABBV-744, respectively) contributed more energy to inhibitor binding than did W81 (−0.96 and −0.85 kcal/mol for ABBV-075 and ABBV-744, respectively). In addition, L94/L387 contributed an energy difference of 0.22 kcal/mol between BD1 and BD2 for ABBV-075/BRD4. In contrast, P82/P375, V87/V380, D88/D381, Y139/Y432, and N140/N433 had over 0.20 kcal/mol of energy difference between BD1 and BD2 for ABBV-744/BRD4 systems. Thus, the conformation needs to be considered to improve selectivity and change the contribution of the same residue sites.

Overall, the selectivity between BRD4-BD1 and BRD4-BD2 was mainly dependent on I146/V439, N140/N433, D144/H437, P82/P375, V87/V380, D88/D381, and Y139/Y432. Regions R3 and R5 of ABBV-075 or ABBV-744 can be employed to improve selectivity between BRD4-BD1 and BRD4-BD2.

3. CONCLUSIONS

BET proteins regulate the expression of several genes and pathways associated with acute myeloid leukemia, acute lymphoblastic leukemia, multiple myeloma, and non-Hodgkin's lymphoma. BD-selective inhibitors have greater effects than pan-BD inhibitors. However, incomplete atomic-level information regarding the pyrrolopyridone core compound/BRD4 interactions has restricted our understanding of the selectivity mechanism for pyrrolopyridone core BET inhibitors. Thus, systematic studies on the pan-BD2 mechanism of pyrrolopyridone analogues using MD simulations and binding free energies are warranted. According to our results, I146 and V439 mainly contributed to the difference between BD1 and BD2 regarding the pyrrolopyridone analogues, whereas additional research using high-precision methods, such as hybrid quantum mechanics/molecular mechanics (QM/MM) simulations, are required to evaluate the roles of D144 and H437. Additionally, the same site residues in BD1 and BD2 contributed to the selectivity mechanism, such as N140/N433, P82/P375, V87/V380, D88/D381, and Y139/Y432. N140/N433 formed hydrogen bonds with the pyrrolopyridone core via the same interactions at different energies. We suggest that the R3 and R5 regions of pyrrolopyridone analogues (such as ABBV-075 and ABBV-744) can be employed to improve the selectivity between BRD4-BD1 and BRD4-BD2 based on the different binding models for pyrrolopyridone analogues. The selectivity mechanism of the pyrrolopyridone analogues

https://doi.org/10.1021/acsomega.3c03935
ACS Omega 2023, 8, 33658−33674

targeting BRD4 was determined based on MD simulations. Nevertheless, the results of our study could be improved by considering water molecules and calculating the edge−to−face interaction between the imidazole ring of H437 and ring D of pyrrolopyridone analogues. In future, other computational tools and experimental methods can be used to design novel pan-BD2 inhibitors and further refine the selectivity mechanism. Furthermore, pan-BD2 inhibitors based on pyrrolopyridone analogues will be designed using molecular docking, MD simulations, binding free energy calculations, kinase, and cellular profiling.

4. METHODS

4.1. Construction Complex Modeling. The ABBV-075/BRD4-BD1 structure was downloaded from the Protein Database Bank (PDB ID:5UVW[79]), and the ABBV-075/BRD4-BD2 complex was obtained by aligning ABBV-075/BRD4-BD1 to pyrrolopyridone compound 18 bound to BRD4-BD2 (PDB ID:6VIX[69]). The method used for constructing the complex system is shown in Figure S89. There are no crystal structures of ABBV-744 binding to human BRD4-BD1 or BRD4-BD2. The crystal complex structures have been published for ABBV-744 binding to BRD2-BD1 and BRD2-BD2 (PDB ID:6ONY[18] and 6E6J,[18] respectively). Thus, the ABBV-744/BRD2-BD1 (ABBV-744/BRD2-BD2) was aligned to structures of BRD4-BD1 with 6VIW[69] (BRD4-BD2 with 6VIX[69]) to construct the ABBV-744/BRD4-BD1 (ABBV-744/BRD4-BD2) complex. Detailed information on these can be found in the Supporting Information.

4.2. MD Simulations. MD simulations were performed on the four complex systems. The force field parameters for ABBV-075 and ABBV-744 were generated using the restrained electrostatic potential protocol[137] and the general amber force field (GAFF, version 2)[138] with the Antechamber module in AMBERTools21.[139] Moreover, the AMBER ff19SB force field[140] was used to define the topological parameters of BRD4-BD1 and BRD4-BD2. Sodium chloride ions were employed to neutralize the inhibitor/BRD4 systems and optimal point-charge water[141] was used to solvate the inhibitor/BET within a 15 Å cuboid box (Table S22). The complex system was minimized in two steps. The Langevin dynamics method was employed to increase the overall system temperature from 0 to 300 K in 200 ps. Next, the isotropic position scaling method was applied to maintain system pressure at 1 bar for 200 ps. Subsequently, the NPT (isothermal-isobaric) ensemble at 200 ps was used to equilibrate the inhibitor/BRD4 system at 300 K and 1 bar. Then, the entire complex system underwent 1000 ns of MD simulations to collect final analysis data. The apo-BRD4-BD1 and apo-BRD4-BD2 systems (without the inhibitors ABBV-075 or ABBV-744) were also subjected to 1000 ns simulations for comparison with the binding systems. Three replicates were used for each system. In total, there were 1000 ns/system/replicate × 8 system × 3 replicates = 24 μs. All simulations were performed using AMBER20.[139] The *CPPTRAJ* module[142,143] was employed to analyze the data from the MD trajectories. Detailed information for the MD simulations is shown in Supporting Information.

4.3. Binding Free Energy. The MM/GBSA approach[144,145] was used to calculate the binding free energies of ABBV-075 and ABBV-744 binding with BRD4-BD1 or BRD4-BD2. The MM/GBSA method is usually used to quantify the binding affinities between small molecules and their target.[146−152] The MM/GBSA framework has been described in detail in previous studies.[153−155] In the present study, the MM/GBSA approach was applied to calculate the energy terms over 1000 frames from the last 100 ns of the MD simulation for the inhibitor/BRD4 complex systems. Additionally, the entropy was calculated via the statistical average with 100 frames in the last 100 ns MS simulation. To determine the contribution of each residue, the binding energy between BRD4 and ABBV-075 (or ABBV-744) was decomposed using MM/GBSA binding energy decomposition without considering entropies.[156] The energy was then calculated using the MMPBA.py program in AMBERTools21.[139] More information regarding the binding free energy calculations is provided in the Supporting Information.

■ ASSOCIATED CONTENT

Supporting Information

The Supporting Information is available free of charge at https://pubs.acs.org/doi/10.1021/acsomega.3c03935.

Details of the method, inhibitor structures, docking results, simulation result analysis, binding free energy, and energy decomposition results (PDF)

■ AUTHOR INFORMATION

Corresponding Authors

Pei Yang − *Department of Hepatobiliary Surgery, Mianyang Central Hospital, School of Medicine, University of Electronic Science and Technology of China, Mianyang 621099 Sichuan, China*; Email: ypppy@126.com

Xiaoan Li − *NHC Key Laboratory of Nuclear Technology Medical Transformation, Mianyang Central Hospital, School of Medicine, University of Electronic Science and Technology of China, Mianyang 621099 Sichuan, China*; orcid.org/0009-0006-8293-8845; Email: lixiaoan@sc-mch.cn

Authors

Mingsong Shi − *NHC Key Laboratory of Nuclear Technology Medical Transformation, Mianyang Central Hospital, School of Medicine, University of Electronic Science and Technology of China, Mianyang 621099 Sichuan, China; Innovation Center of Nursing Research, Nursing Key Laboratory of Sichuan Province, West China Hospital, Sichuan University, Chengdu 610041 Sichuan, China*; orcid.org/0000-0002-8979-5844

Xueting Zheng − *NHC Key Laboratory of Nuclear Technology Medical Transformation, Mianyang Central Hospital, School of Medicine, University of Electronic Science and Technology of China, Mianyang 621099 Sichuan, China*

Yan Zhou − *NHC Key Laboratory of Nuclear Technology Medical Transformation, Mianyang Central Hospital, School of Medicine, University of Electronic Science and Technology of China, Mianyang 621099 Sichuan, China*

Yuan Yin − *NHC Key Laboratory of Nuclear Technology Medical Transformation, Mianyang Central Hospital, School of Medicine, University of Electronic Science and Technology of China, Mianyang 621099 Sichuan, China*

Zhou Lu − *NHC Key Laboratory of Nuclear Technology Medical Transformation, Mianyang Central Hospital, School of Medicine, University of Electronic Science and Technology of China, Mianyang 621099 Sichuan, China*

Zhiyan Zou − *NHC Key Laboratory of Nuclear Technology Medical Transformation, Mianyang Central Hospital, School*

https://doi.org/10.1021/acsomega.3c03935
ACS Omega 2023, 8, 33658−33674

of Medicine, University of Electronic Science and Technology of China, Mianyang 621099 Sichuan, China

Yan Hu − *NHC Key Laboratory of Nuclear Technology Medical Transformation, Mianyang Central Hospital, School of Medicine, University of Electronic Science and Technology of China, Mianyang 621099 Sichuan, China*

Yuanyuan Liang − *NHC Key Laboratory of Nuclear Technology Medical Transformation, Mianyang Central Hospital, School of Medicine, University of Electronic Science and Technology of China, Mianyang 621099 Sichuan, China*

Tingting Chen − *NHC Key Laboratory of Nuclear Technology Medical Transformation, Mianyang Central Hospital, School of Medicine, University of Electronic Science and Technology of China, Mianyang 621099 Sichuan, China*

Yuhan Yang − *NHC Key Laboratory of Nuclear Technology Medical Transformation, Mianyang Central Hospital, School of Medicine, University of Electronic Science and Technology of China, Mianyang 621099 Sichuan, China*

Meng Jing − *Department of Pathology, Mianyang Central Hospital, School of Medicine, University of Electronic Science and Technology of China, Mianyang 621099 Sichuan, China*

Dan Lei − *School of Life Science and Engineering, Southwest University of Science and Technology, Mianyang 621010 Sichuan, China*

Complete contact information is available at: https://pubs.acs.org/10.1021/acsomega.3c03935

Author Contributions

Conceptualization: M.S.; methodology: Y.Z., X.Z., and M.S.; software: M.S. and Y.Y.; validation: Y.Y. and X.Z.; formal analysis: Z.L., X.Z., and Z.Z.; investigation: M.S., Y.Z., X.Z., and Z.Z.; resources: Y.H., D.L., and Y.L.; data curation: T.C., Y.Y., and M.J.; writing—original draft preparation: M.S.; writing—review and editing: M.S., P.Y., and X.L.; visualization: Y.Y., X.Z., Z.Z., and M.S.; supervision: P.Y., M.S., and X.L.; project administration: P.Y. and X.L.; funding acquisition: M.S. and X.L.. All the authors have read and agreed to the published version of the manuscript. M.S. and X.Z. have contributed equally to this work.

Funding

The present work was supported by the National Natural Science Foundation of China (no. 22203056), the Natural Science Foundation of Sichuan, China (no. 2022NSFSC1467), the NHC Key Laboratory of Nuclear Technology Medical Transformation (Mianyang Central Hospital) (no. 2021FH005 and 2022HYX001), and the Foundation of Nursing Key Laboratory of Sichuan Province (no. HLKF2023-(F)-4).

Notes

The authors declare no competing financial interest.

The authors confirm that the data supporting the findings of this study are available within the article and its Supporting Information.

■ ACKNOWLEDGMENTS

Certain data were obtained from the National Supercomputing Center of Guangzhou, the Supercomputing Center of Sichuan University, and the Chengdu Supercomputing Center. The authors thank Editage (www.editage.cn) for English language editing.

■ REFERENCES

(1) Chen, C.; Lu, T.; Chen, P.; Li, Z.; Yang, Y.; Fan, S.; Zhang, Y.; Chen, K.; Fu, W.; Wang, Y.; et al. Cyclization strategy leads to highly potent bromodomain and extra-terminal (bet) bromodomain inhibitors for the treatment of acute liver injury. *Eur. J. Med. Chem.* **2023**, *247*, 115023.

(2) Shen, C. L.; Li, J. L. Lncrna xist silencing protects against sepsis-induced acute liver injury via inhibition of brd4 expression. *Inflammation* **2021**, *44*, 194−205.

(3) Qian, Z.; Shuying, W.; Ranran, D. Inhibitory effects of jq1 on listeria monocytogenes-induced acute liver injury by blocking brd4/ripk1 axis. *Biomed. Pharmacother.* **2020**, *125*, 109818.

(4) Zuber, J.; Shi, J. W.; Wang, E.; Rappaport, A. R.; Herrmann, H.; Sison, E. A.; Magoon, D.; Qi, J.; Blatt, K.; Wunderlich, M.; et al. Rnai screen identifies brd4 as a therapeutic target in acute myeloid leukaemia. *Nature* **2011**, *478*, 524−528.

(5) Khandekar, D.; Tiriveedhi, V. Role of bet inhibitors in triple negative breast cancers. *Cancers* **2020**, *12*, 784.

(6) Zhang, J.; Yang, C.; Tang, P.; Chen, J.; Zhang, D.; Li, Y.; Yang, G.; Liu, Y.; Zhang, Y.; Wang, Y.; et al. Discovery of 4-hydroxyquinazoline derivatives as small molecular bet/parp1 inhibitors that induce defective homologous recombination and lead to synthetic lethality for triple-negative breast cancer therapy. *J. Med. Chem.* **2022**, *65*, 6803−6825.

(7) Ge, J. Y.; Shu, S. K.; Kwon, M.; Jovanović, B.; Murphy, K.; Gulvady, A.; Fassl, A.; Trinh, A.; Kuang, Y. N.; Heavey, G. A.; et al. Acquired resistance to combined bet and cdk4/6 inhibition in triple-negative breast cancer. *Nat. Commun.* **2020**, *11*, 2350.

(8) Liu, L.; Yang, C. J.; Candelario-Jalil, E. Role of bet proteins in inflammation and cns diseases. *Front. Mol. Biosci.* **2021**, *8*, 9.

(9) Wu, C. C.; Cheng, D.; Peng, Y. H.; Li, Y.; Fu, C. Y.; Wang, Y.; Fu, L.; Peng, S. F.; Ni, X. Hepatic brd4 is upregulated in liver fibrosis of various etiologies and positively correlated to fibrotic severity. *Front. Med.* **2021**, *8*, 11.

(10) Salahong, T.; Schwartz, C.; Sungthong, R. Are bet inhibitors yet promising latency-reversing agents for hiv-1 reactivation in aids therapy? *Viruses-Basel* **2021**, *13*, 1026.

(11) Chen, N. C.; Borthakur, G.; Pemmaraju, N. Bromodomain and extra-terminal (bet) inhibitors in treating myeloid neoplasms. *Leuk. Lymphoma* **2021**, *62*, 528−537.

(12) Borck, P. 2C.; Guo, L. W.; Plutzky, J. Bet epigenetic reader proteins in cardiovascular transcriptional programs. *Circ. Res.* **2020**, *126*, 1190−1208.

(13) Plutzky, J. Epigenetic therapeutics for cardiovascular disease writing, erasing, reading, and maybe forgetting. *JAMA-J. Am. Med. Assoc.* **2020**, *323*, 1557−1558.

(14) Taniguchi, Y. The bromodomain and extra-terminal domain (bet) family: Functional anatomy of bet paralogous proteins. *Int. J. Mol. Sci.* **2016**, *17*, 1849.

(15) Gamsjaeger, R.; Webb, S. R.; Lamonica, J. M.; Billin, A.; Blobel, G. A.; Mackay, J. P. Structural basis and specificity of acetylated transcription factor gata1 recognition by bet family bromodomain protein brd3. *Mol. Cell. Biol.* **2011**, *31*, 2632−2640.

(16) Shi, J.; Wang, Y. F.; Zeng, L.; Wu, Y. D.; Deng, J.; Zhang, Q.; Lin, Y. W.; Li, J. L.; Kang, T. B.; Tao, M.; et al. Disrupting the interaction of brd4 with diacetylated twist suppresses tumorigenesis in basal-like breast cancer. *Cancer Cell* **2014**, *25*, 210−225.

(17) Lamonica, J. M.; Deng, W. L.; Kadauke, S.; Campbell, A. E.; Gamsjaeger, R.; Wang, H. X.; Cheng, Y.; Billin, A. N.; Hardison, R. C.; Mackay, J. P.; et al. Bromodomain protein brd3 associates with acetylated gata1 to promote its chromatin occupancy at erythroid target genes. *Proc. Natl. Acad. Sci. U.S.A.* **2011**, *108*, E159−E168.

(18) Faivre, E. J.; McDaniel, K. F.; Albert, D. H.; Mantena, S. R.; Plotnik, J. P.; Wilcox, D.; Zhang, L.; Bui, M. H.; Sheppard, G. S.; Wang, L.; et al. Selective inhibition of the BD2 bromodomain of bet proteins in prostate cancer. *Nature* **2020**, *578*, 306−310.

(19) Gilan, O.; Rioja, I.; Knezevic, K.; Bell, M. J.; Yeung, M. M.; Harker, N. R.; Lam, E. Y. N.; Chung, C. W.; Bamborough, P.; Petretich, M.; et al. Selective targeting of BD1 and BD2 of the bet

proteins in cancer and immunoinflammation. *Science* **2020**, *368*, 387−394.
(20) Preston, A.; Atkinson, S.; Bamborough, P.; Chung, C.-w.; Craggs, P. D.; Gordon, L.; Grandi, P.; Gray, J. R. J.; Jones, E. J.; Lindon, M.; et al. Design and synthesis of a highly selective and in vivo-capable inhibitor of the second bromodomain of the bromodomain and extra terminal domain family of proteins. *J. Med. Chem.* **2020**, *63*, 9070−9092.
(21) Philpott, M.; Rogers, C. M.; Yapp, C.; Wells, C.; Lambert, J. P.; Strain-Damerell, C.; Burgess-Brown, N. A.; Gingras, A. C.; Knapp, S.; Muller, S. Assessing cellular efficacy of bromodomain inhibitors using fluorescence recovery after photobleaching. *Epigenet. Chromatin* **2014**, *7*, 14.
(22) Miller, T. C. R.; Simon, B.; Rybin, V.; Grotsch, H.; Curtet, S.; Khochbin, S.; Carlomagno, T.; Muller, C. W. A bromodomain-DNA interaction facilitates acetylation-dependent bivalent nucleosome recognition by the bet protein brdt. *Nat. Commun.* **2016**, *7*, 13855.
(23) Tyler, D. S.; Vappiani, J.; Caneque, T.; Lam, E. Y. N.; Ward, A.; Gilan, O.; Chan, Y. C.; Hienzsch, A.; Rutkowska, A.; Werner, T.; et al. Click chemistry enables preclinical evaluation of targeted epigenetic therapies. *Science* **2017**, *356*, 1397−1401.
(24) Divakaran, A.; Harki, D. A.; Pomerantz, W. C. K. Recent progress and structural analyses of domain-selective bet inhibitors. *Med. Res. Rev.* **2023**, *43*, 972.
(25) Chen, H. H.; Liu, Z. L.; Zheng, L. L.; Wang, R. R.; Shi, L. Bet inhibitors: An updated patent review (2018-2021). *Expert Opin. Ther. Patents* **2022**, *32*, 953−968.
(26) Schwalm, M. P.; Knapp, S. Bet bromodomain inhibitors. *Curr. Opin. Chem. Biol.* **2022**, *68*, 102148.
(27) Cai, M. H.; Dong, J. Y.; Li, H. B.; Qin, J. J. Recent developments in targeting bromodomain and extra terminal domain proteins for cancer therapeutics. *Curr. Med. Chem.* **2022**, *29*, 4391−4409.
(28) Feng, L.; Wang, G.; Chen, Y.; He, G.; Liu, B.; Liu, J.; Chiang, C. M.; Ouyang, L. Dual-target inhibitors of bromodomain and extra-terminal proteins in cancer: A review from medicinal chemistry perspectives. *Med. Res. Rev.* **2022**, *42*, 710−743.
(29) Groves, A.; Clymer, J.; Filbin, M. G. Bromodomain and extra-terminal protein inhibitors: Biologic insights and therapeutic potential in pediatric brain tumors. *Pharmaceuticals* **2022**, *15*, 665.
(30) Shorstova, T.; Foulkes, W. D.; Witcher, M. Achieving clinical success with bet inhibitors as anti-cancer agents. *Br. J. Cancer* **2021**, *124*, 1478−1490.
(31) Huang, N.; Liao, P.; Zuo, Y.; Zhang, L.; Jiang, R. Design, synthesis, and biological evaluation of a potent dual ezh2-brd4 inhibitor for the treatment of some solid tumors. *J. Med. Chem.* **2023**, *66*, 2646−2662.
(32) Trojer, P. Targeting BET Bromodomains in Cancer. *Ann. Rev. Cancer Biol.* **2022**, *6*, 313−336.
(33) Liu, N.; Ling, R.; Tang, X.; Yu, Y. P.; Zhou, Y. P.; Chen, D. Y. Post-translational modifications of brd4: Therapeutic targets for tumor. *Front. Oncol.* **2022**, *12*, 11.
(34) Jin, W. K.; Tan, H. D.; Wu, J. H.; He, G.; Liu, B. Dual-target inhibitors of bromodomain-containing protein 4 (brd4) in cancer therapy: Current situation and future directions. *Drug Discov. Today* **2022**, *27*, 246−256.
(35) Zhang, Y. H.; Pan, Z. P.; Chen, C.; Tan, Y. W.; Wang, X. Y.; Wang, L.; Zhang, L.; Chen, Y.; He, G. Design, synthesis and anti-ovarian cancer activities of thieno 2,3-d pyrimidine based chimeric brd4 inhibitor/nitric oxide-donator. *Eur. J. Med. Chem.* **2023**, *246*, 114970.
(36) Negri, A.; Marozzi, M.; Trisciuoglio, D.; Rotili, D.; Mai, A.; Rizzi, F. Simultaneous administration of ezh2 and bet inhibitors inhibits proliferation and clonogenic ability of metastatic prostate cancer cells. *J. Enzym. Inhib. Med. Chem.* **2023**, *38*, 11.
(37) Huang, Y. H.; Liu, N.; Pan, Z. Z.; Li, Z.; Sheng, C. Q. Bet-hdac dual inhibitors for combinational treatment of breast cancer and concurrent candidiasis. *J. Med. Chem.* **2023**, *66*, 1239.
(38) Chen, H.; Gesumaria, L.; Park, Y.-K.; Oliver, T. G.; Singer, D. S.; Ge, K.; Schrump, D. S. Bet inhibitors target the sclc-n subtype of small-cell lung cancer by blocking neurod1 transactivation. *Mol. Cancer Res.* **2023**, *21*, 91−101.
(39) Bunnage, M. E.; Chekler, E. L. P.; Jones, L. H. Target validation using chemical probes. *Nat. Chem. Biol.* **2013**, *9*, 195−199.
(40) Song, Y. Q.; Wu, K. J.; Zhang, Z. M.; Liu, T. M.; Ko, C. N.; Zhu, W. G.; Ma, D. L.; Wang, W. H.; Leung, C. H. Development of a sensitive luminescent probe to uncover new brd4 inhibitors in living cells. *Chem. Eng. J.* **2023**, *463*, 142356.
(41) Chekler, E. L. P.; Pellegrino, J. A.; Lanz, T. A.; Denny, R. A.; Flick, A. C.; Coe, J.; Langille, J.; Basak, A.; Liu, S. P.; Stock, I. A.; et al. Transcriptional profiling of a selective creb binding protein bromodomain inhibitor highlights therapeutic opportunities. *Chem. Biol.* **2015**, *22*, 1588−1596.
(42) Gao, Y. Q.; Zhang, J.; Li, J. J.; Song, S. B.; Zhang, S. T.; Liu, Q.; Wang, X.; Zhao, J. B.; Xia, C. C.; Xiao, Y. L.; et al. Establishment of environment-sensitive probes targeting brd3/brd4 for imaging and therapy of tumor. *Eur. J. Med. Chem.* **2023**, *257*, 115478.
(43) Cui, H. R.; Divakaran, A.; Hoell, Z. J.; Ellingson, M. O.; Scholtz, C. R.; Zahid, H.; Johnson, J. A.; Griffith, E. C.; Gee, C. T.; Lee, A. L.; et al. A structure-based design approach for generating high affinity brd4 d1-selective chemical probes. *J. Med. Chem.* **2022**, *65*, 2342.
(44) Bai, P.; Lan, Y.; Wang, H.; Liu, Y.; Striar, R.; Yuan, G. Y.; Afshar, S.; Zagaroli, J. S.; Tocci, D. R.; Langan, A. G.; et al. Synthesis and characterization of a positron emission tomography imaging probe selectively targeting the second bromodomain of bromodomain protein brd4. *Bioconjugate Chem.* **2021**, *32*, 1711−1718.
(45) Bai, P.; Lan, Y.; Patnaik, D.; Wang, H.; Liu, Y.; Chen, Z. D.; Yuan, G. Y.; Afshar, S.; Striar, R.; Zagaroli, J. S.; et al. Design, synthesis, and evaluation of thienodiazepine derivatives as positron emission tomography imaging probes for bromodomain and extra-terminal domain family proteins. *J. Med. Chem.* **2021**, *64*, 14745−14756.
(46) Filippakopoulos, P.; Qi, J.; Picaud, S.; Shen, Y.; Smith, W. B.; Fedorov, O.; Morse, E. M.; Keates, T.; Hickman, T. T.; Felletar, I.; et al. Selective inhibition of bet bromodomains. *Nature* **2010**, *468*, 1067−1073.
(47) Seal, J.; Lamotte, Y.; Donche, F.; Bouillot, A.; Mirguet, O.; Gellibert, F.; Nicodeme, E.; Krysa, G.; Kirilovsky, J.; Beinke, S.; et al. Identification of a novel series of bet family bromodomain inhibitors: Binding mode and profile of i-bet151 (gsk1210151a). *Bioorg. Med. Chem. Lett.* **2012**, *22*, 2968−2972.
(48) Kharenko, O. A.; Patel, R. G.; Calosing, C.; van der Horst, E. H. Combination of zen-3694 with cdk4/6 inhibitors reverses acquired resistance to cdk4/6 inhibitors in er-positive breast cancer. *Cancer Gene Ther.* **2022**, *29*, 859−869.
(49) Aggarwal, R. R.; Schweizer, M. T.; Nanus, D. M.; Pantuck, A. J.; Heath, E. I.; Campeau, E.; Attwell, S.; Norek, K.; Snyder, M.; Bauman, L.; et al. A phase ib/iia study of the pan-bet inhibitor zen-3694 in combination with enzalutamide in patients with metastatic castration-resistant prostate cancer. *Clin. Cancer Res.* **2020**, *26*, 5338−5347.
(50) Pantuck, A. J.; Lee, D. K.; Kee, T.; Wang, P.; Lakhotia, S.; Silverman, M. H.; Mathis, C.; Drakaki, A.; Belldegrun, A. S.; Ho, C. M.; et al. Modulating bet bromodomain inhibitor zen-3694 and enzalutamide combination dosing in a metastatic prostate cancer patient using curate.Ai, an artificial intelligence platform. *Adv. Therap.* **2018**, *1*, 1800104.
(51) Boi, M.; Gaudio, E.; Bonetti, P.; Kwee, I.; Bernasconi, E.; Tarantelli, C.; Rinaldi, A.; Testoni, M.; Cascione, L.; Ponzoni, M.; et al. The bet bromodomain inhibitor otx015 affects pathogenetic pathways in preclinical b-cell tumor models and synergizes with targeted drugs. *Beilstein J. Org. Chem.* **2015**, *21*, 1628−1638.
(52) Noel, J. K.; Iwata, K.; Ooike, S.; Sugahara, K.; Nakamura, H.; Daibata, M. Development of the bet bromodomain inhibitor otx015. *Mol. Cancer Ther.* **2013**, *12*, C244.

https://doi.org/10.1021/acsomega.3c03935
ACS Omega 2023, 8, 33658−33674

(53) Yin, M. Z.; Guo, Y.; Hu, R.; Cai, W. L.; Li, Y.; Pei, S. Y.; Sun, H. Y.; Peng, C.; Li, J. L.; Ye, R.; et al. Potent brd4 inhibitor suppresses cancer cell-macrophage interaction. *Nat. Commun.* **2020**, *11*, 1833.
(54) McDaniel, K. F.; Wang, L.; Soltwedel, T.; Fidanze, S. D.; Hasvold, L. A.; Liu, D. C.; Mantei, R. A.; Pratt, J. K.; Sheppard, G. S.; Bui, M. H.; et al. Discovery of n-(4-(2,4-difluorophenoxy)-3-(6-methyl-7-oxo-6,7-dihydro-1h-pyrrolo 2,3- c pyridin-4-yl)phenyl)-ethanesulfonamide (abbv-075/mivebresib), a potent and orally available bromodomain and extraterminal domain (bet) family bromodomain inhibitor. *J. Med. Chem.* **2017**, *60*, 8369−8384.
(55) Tang, P.; Zhang, J.; Liu, J.; Chiang, C.-M.; Ouyang, L. Targeting bromodomain and extraterminal proteins for drug discovery: From current progress to technological development. *J. Med. Chem.* **2021**, *64*, 2419−2435.
(56) Sun, Y. L.; Han, J.; Wang, Z. Z.; Li, X. N.; Sun, Y. H.; Hu, Z. B. Safety and efficacy of bromodomain and extra-terminal inhibitors for the treatment of hematological malignancies and solid tumors: A systematic study of clinical trials. *Front. Pharmacol* **2021**, *11*, 15.
(57) Divakaran, A.; Scholtz, C. R.; Zahid, H.; Lin, W. W.; Griffith, E. C.; Lee, R. E.; Chen, T. S.; Harki, D. A.; Pomerantz, W. C. K. Development of an n-terminal brd4 bromodomain-targeted degrader. *ACS Med. Chem. Lett.* **2022**, *13*, 1621−1627.
(58) Czerwinska, P.; Mackiewicz, A. A. Bromodomain (brd) family members as regulators of cancer stemness-a comprehensive review. *Int. J. Mol. Sci.* **2023**, *24*, 995.
(59) Zhang, G. T.; Plotnikov, A. N.; Rusinova, E.; Shen, T.; Morohashi, K.; Joshua, J.; Zeng, L.; Mujtaba, S.; Ohlmeyer, M.; Zhou, M. M. Structure-guided design of potent diazobenzene inhibitors for the bet bromodomains. *J. Med. Chem.* **2013**, *56*, 9251−9264.
(60) Gacias, M.; Gerona-Navarro, G.; Plotnikov, A. N.; Zhang, G. T.; Zeng, L.; Kaur, J.; Moy, G.; Rusinova, E.; Rodriguez, Y.; Matikainen, B.; et al. Selective chemical modulation of gene transcription favors oligodendrocyte lineage progression. *Chem. Biol.* **2014**, *21*, 841−854.
(61) Cheung, K. L.; Lu, G. M.; Sharma, R.; Vincek, A.; Zhang, R. H.; Plotnikov, A. N.; Zhang, F.; Zhang, Q.; Ju, Y.; Hu, Y.; et al. Bet n-terminal bromodomain inhibition selectively blocks th17 cell differentiation and ameliorates colitis in mice. *Proc. Natl. Acad. Sci. U.S.A.* **2017**, *114*, 2952−2957.
(62) Ma, J. L.; Chen, H.; Yang, J.; Yu, Z. T.; Huang, P.; Yang, H. F.; Zheng, B. F.; Liu, R. R.; Li, Q. B.; Hu, G. Y.; et al. Binding pocket-based design, synthesis and biological evaluation of novel selective brd4-BD1 inhibitors. *Bioorg. Med. Chem.* **2019**, *27*, 1871−1881.
(63) Liu, Z.; Chen, H.; Wang, P.; Li, Y.; Wold, E. A.; Leonard, P. G.; Joseph, S.; Brasier, A. R.; Tian, B.; Zhou, J. Discovery of orally bioavailable chromone derivatives as potent and selective brd4 inhibitors: Scaffold hopping, optimization, and pharmacological evaluation. *J. Med. Chem.* **2020**, *63*, 5242−5256.
(64) Cui, H. R.; Divakaran, A.; Pandey, A. K.; Johnson, J. A.; Zahid, H.; Hoell, Z. J.; Ellingson, M. O.; Shi, K.; Aihara, H.; Harki, D. A.; et al. Selective n-terminal bet bromodomain inhibitors by targeting non-conserved residues and structured water displacement. *Angew. Chem., Int. Ed.* **2021**, *60*, 1220−1226.
(65) Watson, R. J.; Bamborough, P.; Barnett, H.; Chung, C. W.; Davis, R.; Gordon, L.; Grandi, P.; Petretich, M.; Phillipou, A.; Prinjha, R. K.; et al. Gsk789: A selective inhibitor of the first bromodomains (BD1) of the bromo and extra terminal domain (bet) proteins. *J. Med. Chem.* **2020**, *63*, 9045−9069.
(66) Picaud, S.; Wells, C.; Felletar, I.; Brotherton, D.; Martin, S.; Savitsky, P.; Diez-Dacal, B.; Philpott, M.; Bountra, C.; Lingard, H.; et al. Rvx-208, an inhibitor of bet transcriptional regulators with selectivity for the second bromodomain. *Proc. Natl. Acad. Sci. U.S.A.* **2013**, *110*, 19754−19759.
(67) Law, R. P.; Atkinson, S. J.; Bamborough, P.; Chung, C. W.; Demont, E. H.; Gordon, L. J.; Lindon, M.; Prinjha, R. K.; Watson, A. J. B.; Hirst, D. J. Discovery of tetrahydroquinoxalines as bromodomain and extra-terminal domain (bet) inhibitors with selectivity for the second bromodomain. *J. Med. Chem.* **2018**, *61*, 4317−4334.
(68) Chen, D. H.; Lu, T.; Yan, Z. Q.; Lu, W. C.; Zhou, F.; Lyu, X.; Xu, B.; Jiang, H.; Chen, K.; Luo, C.; et al. Discovery, structural insight, and bioactivities of by27 as a selective inhibitor of the second bromodomains of bet proteins. *Eur. J. Med. Chem.* **2019**, *182*, 111633.
(69) Sheppard, G. S.; Wang, L.; Fidanze, S. D.; Hasvold, L. A.; Liu, D.; Pratt, J. K.; Park, C. H.; Longenecker, K.; Qiu, W.; Torrent, M.; et al. Discovery of n-ethyl-4- 2-(4-fluoro-2,6-dimethyl-phenoxy)-5-(1-hydroxy-1-methyl-ethyl)phenyl -6-methyl-7-oxo-1h-pyrrolo 2,3-c pyridine-2-carboxamide (abbv-744), a bet bromodomain inhibitor with selectivity for the second bromodomain. *J. Med. Chem.* **2020**, *63*, 5585−5623.
(70) Shadrick, W. R.; Slavish, P. J.; Chai, S. C.; Waddell, B.; Connelly, M.; Low, J. A.; Tallant, C.; Young, B. M.; Bharatham, N.; Knapp, S.; et al. Exploiting a water network to achieve enthalpy-driven, bromodomain-selective bet inhibitors. *Bioorg. Med. Chem.* **2018**, *26*, 25−36.
(71) Harrison, L. A.; Atkinson, S. J.; Bassil, A.; Chung, C. W.; Grandi, P.; Gray, J. R. J.; Levernier, E.; Lewis, A.; Lugo, D.; Messenger, C.; et al. Identification of a series of n-methylpyridine-2-carboxamides as potent and selective inhibitors of the second bromodomain (BD2) of the bromo and extra terminal domain (bet) proteins. *J. Med. Chem.* **2021**, *64*, 10742−10771.
(72) Aylott, H. E.; Atkinson, S. J.; Bamborough, P.; Bassil, A.; Chung, C. W.; Gordon, L.; Grandi, P.; Gray, J. R. J.; Harrison, L. A.; Hayhow, T. G.; et al. Template-hopping approach leads to potent, selective, and highly soluble bromo and extraterminal domain (bet) second bromodomain (BD2) inhibitors. *J. Med. Chem.* **2021**, *64*, 3249−3281.
(73) Yu, Z. F.; Ku, A. F.; Anglin, J. L.; Sharma, R.; Ucisik, M. N.; Faver, J. C.; Li, F.; Nyshadham, P.; Simmons, N.; Sharma, K. L.; et al. Discovery and characterization of bromodomain 2-specific inhibitors of brdt. *Proc. Natl. Acad. Sci. U.S.A.* **2021**, *118*, 11.
(74) Burley, S. K.; Bhikadiya, C.; Bi, C. X.; Bittrich, S.; Chao, H.; Chen, L.; Craig, P. A.; Crichlow, G. V.; Dalenberg, K.; Duarte, J. M.; et al. Rcsb protein data bank: Tools for visualizing and understanding biological macromolecules in 3d. *Protein Sci.* **2022**, *31*, 23.
(75) Burley, S. K.; Bhikadiya, C.; Bi, C. X.; Bittrich, S.; Chen, L.; Crichlow, G. V.; Christie, C. H.; Dalenberg, K.; Di Costanzo, L.; Duarte, J. M.; et al. Rcsb protein data bank: Powerful new tools for exploring 3d structures of biological macromolecules for basic and applied research and education in fundamental biology, biomedicine, biotechnology, bioengineering and energy sciences. *Nucleic Acids Res.* **2021**, *49*, D437−D451.
(76) Westbrook, J.; Feng, Z. K.; Chen, L.; Yang, H. W.; Berman, H. M. The protein data bank and structural genomics. *Nucleic Acids Res.* **2003**, *31*, 489−491.
(77) Bui, M. H.; Lin, X. Y.; Albert, D. H.; Li, L. M.; Lam, L. T.; Faivre, E. J.; Warder, S. E.; Huang, X. L.; Wilcox, D.; Donawho, C. K.; et al. Preclinical characterization of bet family bromodomain inhibitor abbv-075 suggests combination therapeutic strategies. *Cancer Res.* **2017**, *77*, 2976−2989.
(78) Piha-Paul, S. A.; Sachdev, J. C.; Barve, M.; LoRusso, P.; Szmulewitz, R.; Patel, S. P.; Lara, P. N.; Chen, X. T.; Hu, B. B.; Freise, K. J.; et al. First-in-human study of mivebresib (abbv-075), an oral pan-inhibitor of bromodomain and extra terminal proteins, in patients with relapsed/refractory solid tumors. *Clin. Cancer Res.* **2019**, *25*, 6309−6319.
(79) Park, C. H. Brd4_bromodomain1-a1376855, 2017. https://www.rcsb.org/structure/5UVW (accessed on March 10, 2023).
(80) Zhao, Z.; Bourne, P. E. Harnessing systematic protein-ligand interaction fingerprints for drug discovery. *Drug Discov. Today* **2022**, *27*, 103319.
(81) Aplin, C.; Milano, S. K.; Zielinski, K. A.; Pollack, L.; Cerione, R. A. Evolving experimental techniques for structure-based drug design. *J. Phys. Chem. B* **2022**, *126*, 6599−6607.
(82) Vyas, V. K.; Bhati, S.; Patel, S.; Ghate, M. Structure- and ligand-based drug design methods for the modeling of antimalarial agents: A review of updates from 2012 onwards. *J. Biomol. Struct. Dyn.* **2022**, *40*, 10481−10506.

https://doi.org/10.1021/acsomega.3c03935
ACS Omega 2023, 8, 33658−33674

(83) Shi, M.; Wang, L.; Li, P.; Liu, J.; Chen, L.; Xu, D. Dasatinib-sik2 binding elucidated by homology modeling, molecular docking, and dynamics simulations. *ACS Omega* **2021**, *6*, 11025−11038.
(84) Lohning, A. E.; Levonis, S. M.; Williams-Noonan, B.; Schweiker, S. S. A practical guide to molecular docking and homology modelling for medicinal chemists. *Curr. Top. Med. Chem.* **2017**, *17*, 2023−2040.
(85) Schmidt, T.; Bergner, A.; Schwede, T. Modelling three-dimensional protein structures for applications in drug design. *Drug Discov. Today* **2014**, *19*, 890−897.
(86) Shi, M.; Zhao, M.; Wang, L.; Liu, K.; Li, P.; Liu, J.; Cai, X.; Chen, L.; Xu, D. Exploring the stability of inhibitor binding to sik2 using molecular dynamics simulation and binding free energy calculation. *Phys. Chem. Chem. Phys.* **2021**, *23*, 13216−13227.
(87) Bhagat, R. T.; Butle, S. R.; Khobragade, D. S.; Wankhede, S. B.; Prasad, C. C.; Mahure, D. S.; Armarkar, A. V. Molecular docking in drug discovery. *J. Pharm. Res. Int.* **2021**, *33*, 46−58.
(88) Chen, G. L.; Seukep, A. J.; Guo, M. Q. Recent advances in molecular docking for the research and discovery of potential marine drugs. *Mar. Drugs* **2020**, *18*, 545.
(89) Zhou, Y.; Li, X.; Luo, P.; Chen, H.; Zhou, Y.; Zheng, X.; Yin, Y.; Wei, H.; Liu, H.; Xia, W.; et al. Identification of abemaciclib derivatives targeting cyclin-dependent kinase 4 and 6 using molecular dynamics, binding free energy calculation, synthesis, and pharmacological evaluation. *Front. Pharmacol* **2023**, *14*, 1154654.
(90) Bunker, A.; Rog, T. Mechanistic understanding from molecular dynamics simulation in pharmaceutical research 1: Drug delivery. *Front. Mol. Biosci.* **2020**, *7*, 36.
(91) Salo-Ahen, O. M. H.; Alanko, I.; Bhadane, R.; Bonvin, A.; Honorato, R. V.; Hossain, S.; Juffer, A. H.; Kabedev, A.; Lahtela-Kakkonen, M.; Larsen, A. S.; et al. Molecular dynamics simulations in drug discovery and pharmaceutical development. *Processes* **2021**, *9*, 71.
(92) Shi, M.; Liu, J.; Fu, S.; Pei, H.; Peng, B.; Wen, Y.; Wei, H.; Zhou, X.; Chen, L.; Xu, D. Structural insights into the interactions of belumosudil with rho-associated coiled-coil containing protein kinases 1 and 2 based on molecular docking, molecular dynamics simulations, and free energy calculations. *J. Comput. Biophys. Chem.* **2023**, *22*, 401.
(93) Shi, M.; Wang, L.; Liu, K.; Chen, Y.; Hu, M.; Yang, L.; He, J.; Chen, L.; Xu, D. Molecular dynamics simulations of the conformational plasticity in the active pocket of salt-inducible kinase 2 (sik2) multi-state binding with bosutinib. *Computational and structural biotechnology journal* **2022**, *20*, 2574−2586.
(94) Nawrocki, G.; Leontyev, I.; Sakipov, S.; Darkhovskiy, M.; Kurnikov, I.; Pereyaslavets, L.; Kamath, G.; Voronina, E.; Butin, O.; Illarionov, A.; et al. Protein-ligand binding free-energy calculations with arrow−a purely first-principles parameterized polarizable force field. *J. Chem. Theory Comput.* **2022**, *18*, 7751−7763.
(95) Blunt, N. S.; Camps, J.; Crawford, O.; Izsak, R.; Leontica, S.; Mirani, A.; Moylett, A. E.; Scivier, S. A.; Sunderhauf, C.; Schopf, P.; et al. Perspective on the current state-of-the-art of quantum computing for drug discovery applications. *J. Chem. Theory Comput.* **2022**, *18*, 7001−7023.
(96) Taylor, A.; Doak, B. C.; Scanlon, M. J. Design of a fragment-screening library. In *Modern Approaches in Drug Discovery*; Lesburg, C. A., Ed.; *Methods in Enzymology*; Elsevier Academic Press Inc, 2018; Vol. *610*, pp 97−115.
(97) Potemkin, V.; Potemkin, A.; Grishina, M. Internet resources for drug discovery and design. *Curr. Top. Med. Chem.* **2018**, *18*, 1955−1975.
(98) Prieto-Martinez, F. D.; Medina-Franco, J. L. Current advances on the development of bet inhibitors: Insights from computational methods. In *Advances in Protein Chemistry and Structural Biology*; KarabenchevaChristova, T., Christov, C., Eds.; *Advances in Protein Chemistry and Structural Biology*; Academic Press Ltd-Elsevier Science Ltd, 2020; Vol. *122*, pp 127−180.
(99) Shi, M. S.; He, J.; Weng, T. T.; Shi, N.; Qi, W. Y.; Guo, Y.; Chen, T.; Chen, L. J.; Xu, D. G. The binding mechanism of nhwd-870 to bromodomain-containing protein 4 based on molecular dynamics simulations and free energy calculation. *Phys. Chem. Chem. Phys.* **2022**, *24*, 5125−5137.
(100) Wang, L. F.; Wang, Y.; Zhao, J.; Yu, Y. X.; Kang, N. Q.; Yang, Z. Y. Theoretical exploration of the binding selectivity of inhibitors to brd7 and brd9 with multiple short molecular dynamics simulations. *RSC Adv.* **2022**, *12*, 16663−16676.
(101) Wu, K. L.; Zhang, C. H.; He, B.; Li, H. X.; Tang, S.; Han, T.; Li, B. K. Virtual screening of antitumor inhibitors targeting brd4 based on machine learning methods. *ChemistrySelect* **2022**, *7*, 6.
(102) Wu, S. L.; Wang, L. F.; Sun, H. B.; Wang, W.; Yu, Y. X. Probing molecular mechanism of inhibitor bindings to bromodomain-containing protein 4 based on molecular dynamics simulations and principal component analysis. *SAR QSAR Environ. Res.* **2020**, *31*, 547−570.
(103) Zhong, H. Y.; Wang, Z.; Wang, X. W.; Liu, H.; Li, D.; Liu, H. X.; Yao, X. J.; Hou, T. J. Importance of a crystalline water network in docking-based virtual screening: A case study of brd4. *Phys. Chem. Chem. Phys.* **2019**, *21*, 25276−25289.
(104) Su, J.; Liu, X. G.; Zhang, S. L.; Yan, F. F.; Zhang, Q. G.; Chen, J. Z. A theoretical insight into selectivity of inhibitors toward two domains of bromodomain-containing protein 4 using molecular dynamics simulations. *Chem. Biol. Drug Des.* **2018**, *91*, 828−840.
(105) Aldeghi, M.; Ross, G. A.; Bodkin, M. J.; Essex, J. W.; Knapp, S.; Biggin, P. C. Large-scale analysis of water stability in bromodomain binding pockets with grand canonical monte carlo. *Comm. Chem.* **2018**, *1*, 19.
(106) Aldeghi, M.; Heifetz, A.; Bodkin, M. J.; Knapp, S.; Biggin, P. C. Accurate calculation of the absolute free energy of binding for drug molecules. *Chem. Sci.* **2016**, *7*, 207−218.
(107) Ran, T.; Zhang, Z. M.; Liu, K. J.; Lu, Y.; Li, H. F.; Xu, J. X.; Xiong, X.; Zhang, Y. M.; Xu, A. Y.; Lu, S.; et al. Insight into the key interactions of bromodomain inhibitors based on molecular docking, interaction fingerprinting, molecular dynamics and binding free energy calculation. *Mol. Biosyst.* **2015**, *11*, 1295−1304.
(108) Kuang, M.; Zhou, J. W.; Wang, L. Y.; Liu, Z. H.; Guo, J.; Wu, R. B. Binding kinetics versus affinities in brd4 inhibition. *J. Chem. Inf. Model.* **2015**, *55*, 1926−1935.
(109) Su, J.; Liu, X. G.; Zhang, S. L.; Yan, F. F.; Zhang, Q. G.; Chen, J. Z. Insight into selective mechanism of class of i-brd9 inhibitors toward brd9 based on molecular dynamics simulations. *Chem. Biol. Drug Des.* **2019**, *93*, 163−176.
(110) Raich, L.; Meier, K.; Gunther, J.; Christ, C. D.; Noe, F.; Olsson, S. Discovery of a hidden transient state in all bromodomain families. *Proc. Natl. Acad. Sci. U.S.A.* **2021**, *118*, 7.
(111) Tumdam, R.; Kumar, A.; Subbarao, N.; Balaji, B. S. In silico study directed towards identification of novel high-affinity inhibitors targeting an oncogenic protein: Brd4-BD1. *SAR QSAR Environ. Res.* **2018**, *29*, 975−996.
(112) Zhang, X. X.; Chen, K.; Wu, Y. D.; Wiest, O. Protein dynamics and structural waters in bromodomains. *PLoS One* **2017**, *12*, No. e0186570.
(113) Cheng, C. Y.; Diao, H. J.; Zhang, F.; Wang, Y. H.; Wang, K.; Wu, R. B. Deciphering the mechanisms of selective inhibition for the tandem BD1/BD2 in the bet-bromodomain family. *Phys. Chem. Chem. Phys.* **2017**, *19*, 23934−23941.
(114) Weiser, J.; Shenkin, P. S.; Still, W. C. Approximate atomic surfaces from linear combinations of pairwise overlaps (lcpo). *J. Comput. Chem.* **1999**, *20*, 217−230.
(115) Li, J.; Zou, W.; Yu, K. K.; Liu, B.; Liang, W. F.; Wang, L. S.; Lu, Y.; Jiang, Z. Q.; Wang, A. Y.; Zhu, J. P. Discovery of the natural product 3 ',4 ',7,8-tetrahydroxyflavone as a novel and potent selective brd4 bromodomain 2 inhibitor. *J. Enzym. Inhib. Med. Chem.* **2021**, *36*, 903−913.
(116) Kong, B.; Zhu, Z. H.; Li, H. M.; Hong, Q. Q.; Wang, C.; Ma, Y.; Zheng, W.; Jiang, F.; Zhang, Z. M.; Ran, T.; et al. Discovery of 1-(5-(1h-benzo d imidazole-2-yl)-2,4-dimethyl-1h-pyrrol-3-yl)ethan-1-one derivatives as novel and potent bromodomain and extra-terminal (bet) inhibitors with anticancer efficacy. *Eur. J. Med. Chem.* **2022**, *227*, 113953.

https://doi.org/10.1021/acsomega.3c03935
ACS Omega 2023, 8, 33658−33674

(117) Zhao, L.; Cao, D.; Chen, T.; Wang, Y.; Miao, Z.; Xu, Y.; Chen, W.; Wang, X.; Li, Y.; Du, Z.; et al. Fragment-based drug discovery of 2-thiazolidinones as inhibitors of the histone reader brd4 bromodomain. *J. Med. Chem.* **2013**, *56*, 3833−3851.
(118) Zhang, M. F.; Zhang, Y.; Song, M.; Xue, X. Q.; Wang, J. J.; Wang, C.; Zhang, C.; Li, C. C.; Xiang, Q. P.; Zou, L. J.; et al. Structure-Based Discovery and Optimization of Benzo[*d*]isoxazole Derivatives as Potent and Selective BET Inhibitors for Potential Treatment of Castration-Resistant Prostate Cancer (CRPC). *J. Med. Chem.* **2018**, *61*, 3037−3058.
(119) Xue, X. Q.; Zhang, Y.; Liu, Z. X.; Song, M.; Xing, Y. L.; Xiang, Q. P.; Wang, Z.; Tu, Z. C.; Zhou, Y. L.; Ding, K.; et al. Discovery of benzo cd indol-2(1h)-ones as potent and specific bet bromodomain inhibitors: Structure-based virtual screening, optimization, and biological evaluation. *J. Med. Chem.* **2016**, *59*, 1565−1579.
(120) Wellaway, C. R.; Bamborough, P.; Bernard, S. G.; Chung, C. W.; Craggs, P. D.; Cutler, L.; Demont, E. H.; Evans, J. P.; Gordon, L.; Karamshi, B.; et al. Structure-based design of a bromodomain and extraterminal domain (bet) inhibitor selective for the n-terminal bromodomains that retains an anti-inflammatory and antiproliferative phenotype. *J. Med. Chem.* **2020**, *63*, 9020−9044.
(121) Xing, L.; Klug-Mcleod, J.; Rai, B.; Lunney, E. A. Kinase hinge binding scaffolds and their hydrogen bond patterns. *Bioorg. Med. Chem.* **2015**, *23*, 6520−6527.
(122) Kenny, P. W. Hydrogen-bond donors in drug design. *J. Med. Chem.* **2022**, *65*, 14261−14275.
(123) Bulusu, G.; Desiraju, G. R. Strong and weak hydrogen bonds in protein-ligand recognition. *J. Indian Inst. Sci.* **2020**, *100*, 31−41.
(124) Caron, G.; Kihlberg, J.; Ermondi, G. Intramolecular hydrogen bonding: An opportunity for improved design in medicinal chemistry. *Med. Res. Rev.* **2019**, *39*, 1707−1729.
(125) Li, J. H.; Zhang, C.; Xu, H. R.; Wang, C.; Dong, R. B.; Shen, H.; Zhuang, X. X.; Chen, X. S.; Li, Q.; Lu, J. B.; et al. Structure-based discovery and optimization of furo 3,2-c pyridin-4(5h)-one derivatives as potent and second bromodomain (BD2)-selective bromo and extra terminal domain (bet) inhibitors br. *J. Med. Chem.* **2022**, *65*, 5760−5799.
(126) Jennings, L. E.; Schiedel, M.; Hewings, D. S.; Picaud, S.; Laurin, C. M. C.; Bruno, P. A.; Bluck, J. P.; Scorah, A. R.; See, L.; Reynolds, J. K.; et al. Bet bromodomain ligands: Probing the wpf shelf to improve brd4 bromodomain affinity and metabolic stability. *Bioorg. Med. Chem.* **2018**, *26*, 2937−2957.
(127) Wang, L.; Pratt, J. K.; Soltwedel, T.; Sheppard, G. S.; Fidanze, S. D.; Liu, D. C.; Hasvold, L. A.; Mantei, R. A.; Holms, J. H.; McClellan, W. J.; et al. Fragment-based, structure-enabled discovery of novel pyridones and pyridone macrocycles as potent bromodomain and extra-terminal domain (bet) family bromodomain inhibitors. *J. Med. Chem.* **2017**, *60*, 3828−3850.
(128) Hasvold, L. A.; Sheppard, G. S.; Wang, L.; Fidanze, S. D.; Liu, D. C.; Pratt, J. K.; Mantei, R. A.; Wada, C. K.; Hubbard, R.; Shen, Y.; et al. Methylpyrrole inhibitors of bet bromodomains. *Bioorg. Med. Chem. Lett.* **2017**, *27*, 2225−2233.
(129) Chen, J. J.; Li, Y. L.; Zhang, J.; Zhang, M. M.; Wei, A. H.; Liu, H. C.; Xie, Z. C.; Ren, W. M.; Duan, W. W.; Zhang, Z.; et al. Discovery of selective hdac/brd4 dual inhibitors as epigenetic probes. *Eur. J. Med. Chem.* **2021**, *209*, 112868.
(130) Asai, D.; Inoue, N.; Sugiyama, M.; Fujita, T.; Matsuyama, Y.; Liu, X. H.; Matsushima, A.; Nose, T.; Costa, T.; Shimohigashi, Y. Direct evidence of edge-to-face ch/pi interaction for par-1 thrombin receptor activation. *Bioorg. Med. Chem.* **2021**, *51*, 116498.
(131) Eto, M.; Yamaguchi, K.; Shinohara, I.; Ito, F.; Yoshitake, Y.; Harano, K. Role of edge-to-face interaction between aromatic rings in clathrate formation of 1-benzoyl-2-hydroxyindoline derivatives with benzene. X-ray crystal and pm6 analyses of the interaction. *Tetrahedron* **2011**, *67*, 7400−7405.
(132) Sukalovic, V. V.; Zlatović, M. V.; Roglic, G. M.; Kostic-Rajacic, S. V.; Andric, D. B. Application of hybrid density functional theory in calculation of edge-to-face interactions of receptor-ligand system. *Acta Chim. Slov.* **2009**, *56*, 270−277.
(133) Ercolani, G.; Mencarelli, P. Role of face-to-face and edge-to-face aromatic interactions in the inclusion complexation of cyclobis-(paraquat-p-phenylene): A theoretical study. *J. Org. Chem.* **2003**, *68*, 6470−6473.
(134) Sheppard, G. S.; Wang, L.; Fidanze, S. D.; Hasvold, L. A.; Liu, D. C.; Pratt, J. K.; Park, C. H.; Bui, M.-H.; Faivre, E. J.; Huang, X. L.; et al. Discovery of abbv-744, a first-in-class highly bdii-selective bet bromodomain inhibitor. *Cancer Res.* **2018**, *78*, 931.
(135) Wang, L.; Sheppard, G.; Fidanze, S.; Hasvold, L.; Liu, D. C.; Pratt, J.; Bui, M. H.; Faivre, E.; Huang, X. L.; Lin, X.; et al. Structure based design: Identification of the clinical candidate abbv-744, a first-in-class highly bdii-selective bet bromodomain inhibitor. *Abstr. Pap. Am. Chem. Soc.* **2018**, *256*, 1.
(136) Lin, X. Y.; Huang, X. L.; Bellin, R.; Faivre, E.; Hessler, P.; Lam, L.; Bui, M. H.; Wilcox, D.; Uziel, T.; Ferguson, D. C.; et al. Abbv-744, a first-in-class and highly selective inhibitor of the second bromodomain of bet family proteins, displays robust activities in preclinical models of acute myelogenous leukemia. *Cancer Res.* **2018**, *78*, 800.
(137) Bayly, C. I.; Cieplak, P.; Cornell, W. D.; Kollman, P. A. A well-behaved electrostatic potential based method using charge restraints for deriving atomic charges: The resp model. *J. Phys. Chem.* **1993**, *97*, 10269−10280.
(138) Wang, J. M.; Wolf, R. M.; Caldwell, J. W.; Kollman, P. A.; Case, D. A. Development and testing of a general amber force field. *J. Comput. Chem.* **2004**, *25*, 1157−1174.
(139) *Amber 2020*; University of California: San Francisco, 2020. (accessed).
(140) Tian, C.; Kasavajhala, K.; Belfon, K. A. A.; Raguette, L.; Huang, H.; Migues, A. N.; Bickel, J.; Wang, Y. Z.; Pincay, J.; Wu, Q.; et al. Ff19sb: Amino-acid-specific protein backbone parameters trained against quantum mechanics energy surfaces in solution. *J. Chem. Theory Comput.* **2020**, *16*, 528−552.
(141) Izadi, S.; Anandakrishnan, R.; Onufriev, A. V. Building water models: A different approach. *J. Phys. Chem. Lett.* **2014**, *5*, 3863−3871.
(142) Cheatham, T.; Galindo, R.; Roe, D. Parallel analysis of large ensembles of molecular dynamics simulation derived trajectories with the open-source cpptraj tools. *Abstracts of Papers of the American Chemical Society* **2019**, *257*, 1.
(143) Roe, D. R.; Cheatham, T. E. Parallelization of cpptraj enables large scale analysis of molecular dynamics trajectory data. *J. Comput. Chem.* **2018**, *39*, 2110−2117.
(144) Srinivasan, J.; Cheatham, T. E.; Cieplak, P.; Kollman, P. A.; Case, D. A. Continuum solvent studies of the stability of DNA, rna, and phosphoramidate - DNA helices. *J. Am. Chem. Soc.* **1998**, *120*, 9401−9409.
(145) Lee, M. S.; Salsbury, F. R.; Olson, M. A. An efficient hybrid explicit/implicit solvent method for biomolecular simulations. *J. Comput. Chem.* **2004**, *25*, 1967−1978.
(146) Shi, M.; Xu, D. Molecular dynamics investigations suggest a non-specific recognition strategy of 14-3-3σ protein by tweezer: Implication for the inhibition mechanism. *Front. Chem.* **2019**, *7*, 237.
(147) Wang, J. Y.; Chen, Q.; Wang, M.; Zhong, C. The opening/closure of the p-loop and hinge of bcr-abl1 decodes the low/high bioactivities of dasatinib and axitinib. *Phys. Chem. Chem. Phys.* **2017**, *19*, 22444−22453.
(148) Tse, A.; Verkhivker, G. M. Molecular dynamics simulations and structural network analysis of c-abl and c-src kinase core proteins: Capturing allosteric mechanisms and communication pathways from residue centrality. *J. Chem. Inf. Model.* **2015**, *55*, 1645−1662.
(149) Xu, D.; Zheng, Q. C. Theoretical investigations on the effects of mutations in important residues of ns1b on its rna-binding using molecular dynamics simulations. *Comput. Biol. Med.* **2022**, *145*, 105412.
(150) Chen, Q. Q.; Wang, Y.; Shi, S. S.; Li, K. H.; Zhang, L.; Gao, J. Insights into the interaction mechanisms of the proviral integration site of moloney murine leukemia virus (pim) kinases with pan-pim

https://doi.org/10.1021/acsomega.3c03935
ACS Omega 2023, 8, 33658−33674

inhibitors pim447 and azd1208: A molecular dynamics simulation and mm/gbsa calculation study. *Int. J. Mol. Sci.* **2019**, *20*, 5410.
(151) Wei, W. Q.; Chen, Y. N.; Xie, D. Q.; Zhou, Y. Z. Molecular insight into chymotrypsin inhibitor 2 resisting proteolytic degradation. *Phys. Chem. Chem. Phys.* **2019**, *21*, 5049−5058.
(152) Chen, J. Z.; Zeng, Q. K.; Wang, W.; Sun, H. B.; Hu, G. D. Decoding the identification mechanism of an sam-iii riboswitch on ligands through multiple independent gaussian-accelerated molecular dynamics simulations. *J. Chem. Inf. Model.* **2022**, *62*, 6118−6132.
(153) Honig, B.; Nicholls, A. Classical electrostatics in biology and chemistry. *Science* **1995**, *268*, 1144−1149.
(154) Genheden, S.; Ryde, U. The mm/pbsa and mm/gbsa methods to estimate ligand-binding affinities. *Expert. Opin. Drug Discov.* **2015**, *10*, 449−461.
(155) Onufriev, A. V.; Case, D. A. Generalized born implicit solvent models for biomolecules. In *Annual Review of Biophysics, vol 48*; Dill, K. A., Ed.; *Annual Review of Biophysics*; Annual Reviews, 2019; Vol. *48*, pp 275−296.
(156) Gaillard, T.; Simonson, T. Pairwise decomposition of an mmgbsa energy function for computational protein design. *J. Comput. Chem.* **2014**, *35*, 1371−1387.

https://doi.org/10.1021/acsomega.3c03935
ACS Omega 2023, 8, 33658−33674